Human Molecular Genetics, 2018, Vol. 27, No. 4 716–731

doi: 10.1093/hmg/ddx437
Advance Access Publication Date: 21 December 2017
Original Article

ORIGINAL ARTICLE

Smchd1 haploinsufficiency exacerbates the phenotype of a transgenic FSHD1 mouse model

Jessica C. de Greef[1,†], Yvonne D. Krom[1,†,¶], Bianca den Hamer[1], Lauren Snider[2], Yosuke Hiramuki[2], Rob F.P. van den Akker[1], Kelsey Breslin[3], Miha Pakusch[3], Daniela C.F. Salvatori[4], Bram Slütter[5], Rabi Tawil[6], Marnie E. Blewitt[3,7,‡], Stephen J. Tapscott[2,‡] and Silvère M. van der Maarel[1,*]

[1]Department of Human Genetics, Leiden University Medical Center, Leiden, The Netherlands, [2]Division of Human Biology, Fred Hutchinson Cancer Research Center, Seattle, WA, USA, [3]The Walter and Eliza Hall Institute of Medical Research, Melbourne, Australia, [4]Central Laboratory Animal Facility, Leiden University Medical Center, [5]Divisions of Biopharmaceutics & Drug Delivery Technology, Leiden Academic Centre for Drug Research (LACDR), Leiden University, Leiden, The Netherlands, [6]Neuromuscular Disease Unit, Department of Neurology, University of Rochester Medical Center, Rochester, NY, USA and [7]University of Melbourne, Melbourne, Australia

*To whom correspondence should be addressed at: Department of Human Genetics, Leiden University Medical Center, Albinusdreef 2, 2333 ZA Leiden, The Netherlands. Tel: +31 715269480; Fax: +31 715268285. Email: s.m.van_der_maarel@lumc.nl

Abstract

In humans, a copy of the *DUX4* retrogene is located in each unit of the D4Z4 macrosatellite repeat that normally comprises 8–100 units. The D4Z4 repeat has heterochromatic features and does not express DUX4 in somatic cells. Individuals with facioscapulohumeral muscular dystrophy (FSHD) have a partial failure of somatic DUX4 repression resulting in the presence of DUX4 protein in sporadic muscle nuclei. Somatic DUX4 derepression is caused by contraction of the D4Z4 repeat to 1–10 units (FSHD1) or by heterozygous mutations in genes responsible for maintaining the D4Z4 chromatin structure in a repressive state (FSHD2). One of the FSHD2 genes is the structural maintenance of chromosomes hinge domain 1 (*SMCHD1*) gene. *SMCHD1* mutations have also been identified in FSHD1; patients carrying a contracted D4Z4 repeat and a *SMCHD1* mutation are more severely affected than relatives with only a contracted repeat or a *SMCHD1* mutation. To evaluate the modifier role of SMCHD1, we crossbred mice carrying a contracted D4Z4 repeat (D4Z4–2.5 mice) with mice that are haploinsufficient for Smchd1 (Smchd1^{MommeD1} mice). D4Z4–2.5/Smchd1^{MommeD1} mice presented with a significantly reduced body weight and developed skin lesions. The same skin lesions, albeit in a milder form, were also observed in D4Z4–2.5 mice, suggesting that reduced Smchd1 levels aggravate disease in the D4Z4–2.5 mouse model. Our study emphasizes the evolutionary conservation of the SMCHD1-dependent epigenetic regulation of the D4Z4 repeat array and further suggests that the D4Z4–2.5/Smchd1^{MommeD1} mouse model may be used to unravel the function of DUX4 in non-muscle tissues like the skin.

[†]The authors wish it to be known that, in their opinion, the first two authors should be regarded as joint First Authors.
[‡]These authors contributed equally to this work.
[¶]Present address: Department of Neurology, Leiden University Medical Center, Leiden, The Netherlands.
Received: November 11, 2017. **Revised:** December 9, 2017. **Accepted:** December 18, 2017

Introduction

DUX4 is a double homeobox transcription factor expressed in the luminal cells of the testis (1) and in cleavage stage embryos (2–4). A copy of the *DUX4* retrogene is located in each unit of the D4Z4 macrosatellite repeat at the subtelomere of chromosome 4q. This D4Z4 repeat is polymorphic in size and typically consists of 8–100 D4Z4 repeat units (5–7). In most somatic cells, the D4Z4 repeat has heterochromatic features and, likely due to repeat-mediated epigenetic repression, does not express or rarely expresses DUX4 (1,8–10). Individuals with FSHD, a common inherited myopathy that initially affects muscles of the face, shoulder girdle, and upper arms, have a partial failure of the epigenetic repression of the D4Z4 repeat, resulting in the presence of DUX4 protein in a limited number of muscle nuclei (1). This failure in epigenetic repression can be caused by contraction of the D4Z4 repeat to 1–10 units (FSHD1) (5,6), by heterozygous mutations in the *SMCHD1* gene (FSHD2) (11), or in rare cases by heterozygous mutations in the DNA methyltransferase 3B (*DNMT3B*) gene (FSHD2) (12). *SMCHD1* and *DNMT3B* both encode chromatin modifiers that seem to be necessary to establish and/or maintain a repressive chromatin structure of the D4Z4 repeat in somatic cells. *SMCHD1* and *DNMT3B* mutations have also been identified in FSHD1 families; patients that carry both a contracted D4Z4 repeat and a FSHD2 mutation present with a more severe clinical phenotype than relatives carrying only the D4Z4 repeat contraction or the *SMCHD1*/*DNMT3B* mutation (12–14). In agreement, enhanced *DUX4* transcript levels were measured in myotube cultures from FSHD1 patients upon SMCHD1 knockdown (13).

To study the *in vivo* epigenetic regulation of the D4Z4 repeat locus, we previously generated hemizygous transgenic mice carrying either a control-sized D4Z4 repeat (D4Z4–12.5 mice) or a FSHD-sized D4Z4 repeat (D4Z4–2.5 mice) (15). In these mice, we demonstrated that the mechanism of epigenetic repression of DUX4 in somatic cells seems to be conserved between mice and man. Control D4Z4–12.5 mice present with DUX4 expression in the germline, but DUX4 is epigenetically repressed in somatic cells. In contrast, D4Z4–2.5 mice fail to efficiently repress DUX4 in somatic cells. As a consequence, sporadic muscle nuclei express relatively abundant amounts of DUX4 protein (15). Though the FSHD molecular hallmarks are conserved in D4Z4–2.5 mice, we questioned whether modelling FSHD in rodents will elicit the same pathological consequences as in human. This is supported by the notion that, apart from an uncharacterized eye phenotype, D4Z4–2.5 mice appear healthy without obvious signs of a muscular dystrophy phenotype (15). However, DUX4 overexpression by intramuscular injection with AAV6-DUX4 in mouse skeletal muscle does lead to muscle damage (16). In addition, a novel FSHD mouse model with muscle-specific doxycycline-regulated DUX4 expression presents with a slow progressive degenerative myopathy involving inflammation and fibrosis (17). The relatively low levels of DUX4 RNA and protein in skeletal muscle in the D4Z4–2.5 mouse model may explain the lack of muscle pathology in these mice. Furthermore, DUX4 protein expression in D4Z4–2.5 mice is restricted to Myog-negative myoblasts, which do not fuse into myotubes (15). In contrast, in FSHD patients DUX4 protein expression is observed in myosin-positive myotubes (18,19). Thus, the transgene spatial and temporal expression pattern may explain the failure of modelling the FSHD muscle phenotype in our D4Z4–2.5 mice.

In the current study, we modelled the digenic requirements of FSHD by crossbreeding D4Z4–2.5 mice with mice that are haploinsufficient for Smchd1 (Smchd1^{MommeD1} mice), and we evaluated the modifier role of Smchd1 on disease severity. The Smchd1^{MommeD1} mutation, a nonsense *Smchd1* mutation in exon 23 (p.Q963X), was identified in an *N*-ethyl-*N*-nitrosourea mutagenesis screen for modifiers of epigenetic reprogramming (20). *Smchd1* encodes a well-conserved protein with a C-terminal SMC hinge domain and an N-terminal ATPase domain. In mice, Smchd1 has roles in the establishment and/or maintenance of DNA methylation, in X chromosome inactivation, and in the regulation of some clustered and imprinted genes (21–23). However, its exact function is still unknown. Smchd1^{MommeD1} homozygous females die between E9.5 and E11.5, and lack DNA methylation at many X-linked genes, including *Hprt1*. In contrast, some homozygous males and all heterozygous males and females survive, the latter presenting with normal *Hprt1* DNA methylation levels by adulthood (20,21).

In this study, we show that Smchd1 haploinsufficiency results in decreased Smchd1 transcript levels with consequences for the chromatin structure of the D4Z4 transgene in the D4Z4–2.5 mouse model. In addition, reduced Smchd1 expression seems to affect specific tissues, most notably the skin and the thymus. D4Z4–2.5/Smchd1^{MommeD1} mice present with significantly increased DUX4 transcript levels in muzzle skin and thymus leading to a skin phenotype starting from postnatal day 10 and a severely reduced body weight from postnatal day 12. Similar, but much milder, skin lesions are also observed in D4Z4–2.5 mice. This mouse model is not the first DUX4 expressing mouse model with a skin and a runting phenotype. The iDUX4 (2.7) mouse carries a doxycycline-inducible DUX4 transgene and presents with a skin phenotype consisting of increased epidermal thickness and nuclear dermal density and the carrier males that survived to birth were severely runted (24). Importantly, Smchd1 haploinsufficiency does not seem to impact skeletal muscle. DUX4 transcript levels are not or only slightly increased in skeletal muscles of D4Z4–2.5/Smchd1^{MommeD1} mice compared with D4Z4–2.5 mice. Also, the skeletal muscles of the D4Z4–2.5/Smchd1^{MommeD1} mice do not show overt muscle pathology. In conclusion, the D4Z4–2.5 mice and the D4Z4–2.5/Smchd1^{MommeD1} mice can be used to study the epigenetic regulation of the D4Z4 repeat array. Furthermore, the D4Z4–2.5/Smchd1^{MommeD1} mouse model may be suitable to study the function of DUX4 in the skin and the thymus.

Results

Smchd1 haploinsufficiency affects *Smchd1* transcript levels, D4Z4 chromatin structure, and potentially DUX4 expression

We showed previously that SMCHD1 binds the D4Z4 repeat in human fibroblast cultures (11). To determine whether mouse Smchd1 binds the human D4Z4 transgene in the D4Z4–2.5 mouse model, we performed Smchd1 chromatin immunoprecipitation (ChIP) analysis in fibroblasts isolated from three neonatal D4Z4–2.5 mice. This was indeed the case (Fig. 1A), and we concluded that D4Z4–2.5 mice are a suitable model to evaluate the modifier role of Smchd1 on D4Z4 chromatin structure, DUX4 expression, and disease severity. Next, we determined the effect of the Smchd1^{MommeD1} mutation on *Smchd1* expression in D4Z4–2.5 mice by crossbreeding a heterozygous Smchd1^{MommeD1} male mouse with a hemizygous D4Z4–2.5 female mouse. We then observed that *Smchd1* transcript levels were significantly reduced in all tissues tested of hemizygous D4Z4–2.5 mice carrying

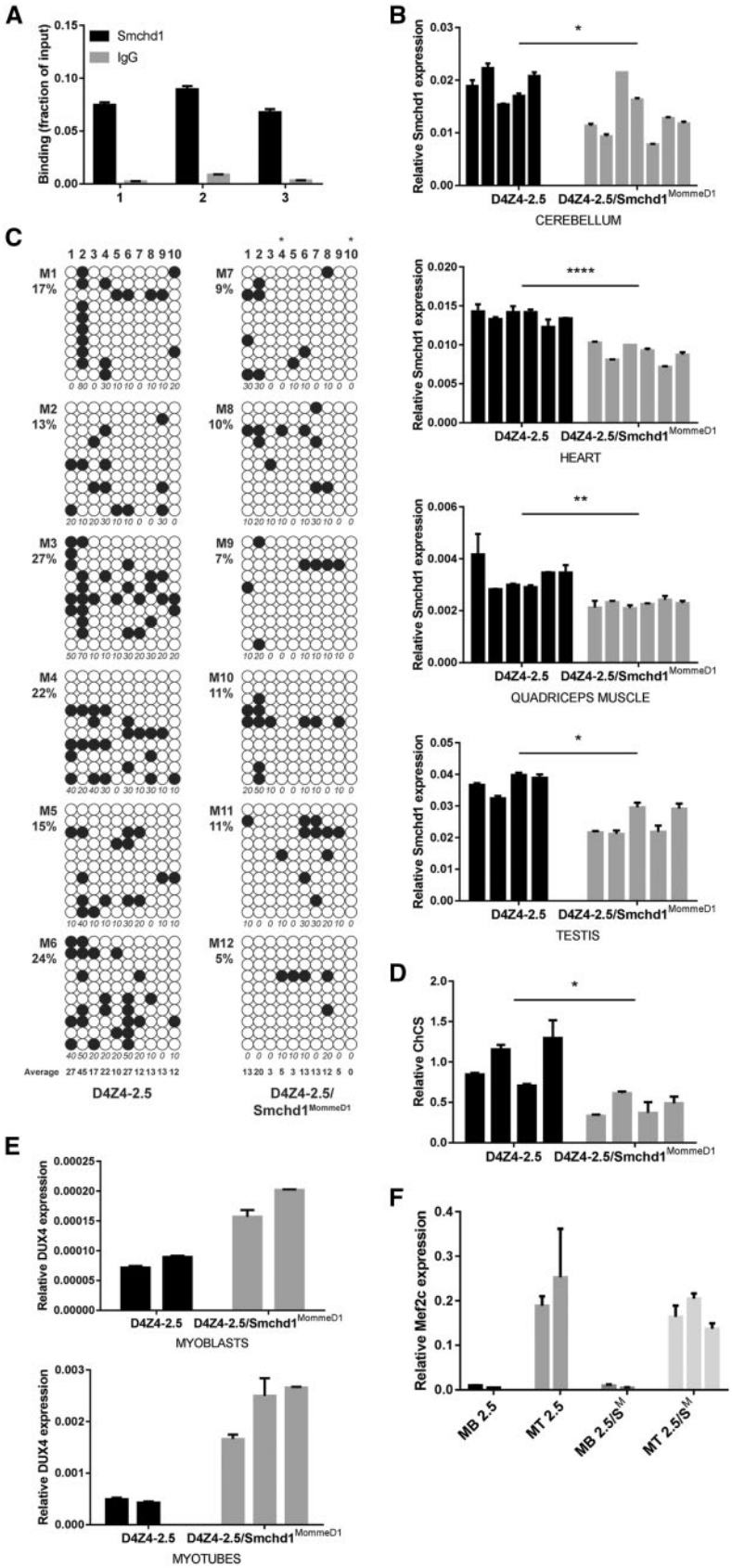

Figure 1. Smchd1 haploinsufficiency affects *Smchd1* transcript levels, D4Z4 chromatin structure, and potentially DUX4 expression. (**A**) Mouse Smchd1 binds the D4Z4 transgene in fibroblasts isolated from three neonatal D4Z4-2.5 mice, as tested by ChIP-qPCR analysis. (**B**) Relative *Smchd1* expression in cerebellum, heart, quadriceps muscle, and testis of D4Z4-2.5 and D4Z4-2.5/Smchd1^{MommeD1} mice (postnatal day 15). Statistical analysis was performed on the average *Smchd1* expression in each mouse using Student's *t*-test (cerebellum, heart, quadriceps muscle) or Mann–Whitney *U* test (testis). *P<0.05; **P<0.01; ****P<0.0001. (**C**) DNA methylation levels were

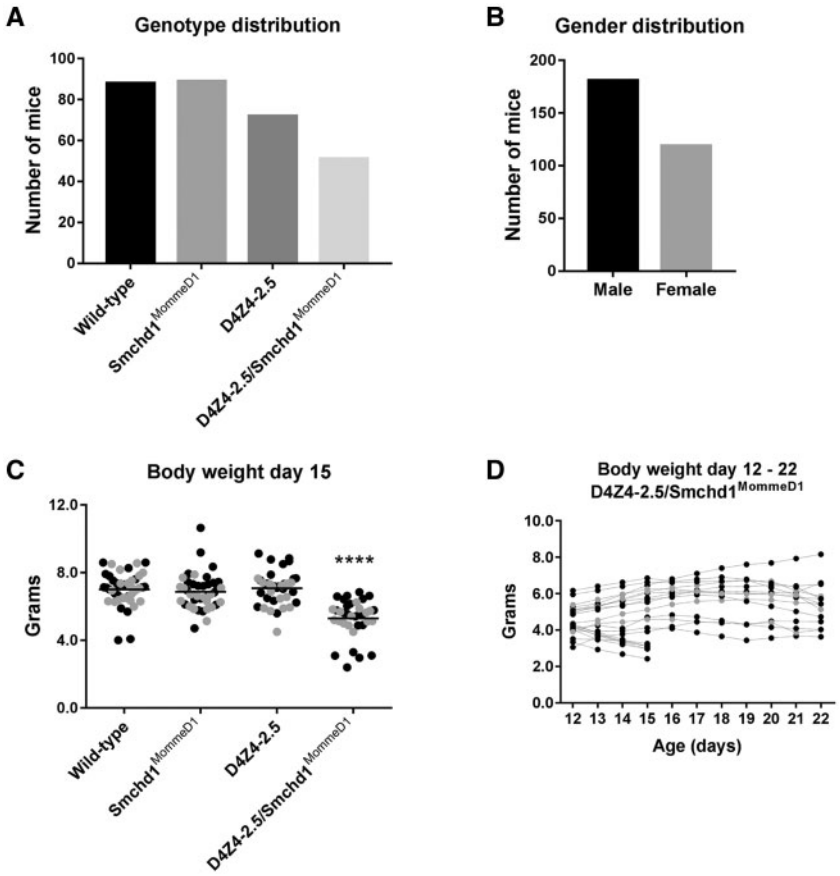

Figure 2. Genotype distribution, gender distribution, and body weight are distorted in mice born from D4Z4–2.5/Smchd1^{MommeD1} crossbreedings. (**A**) Genotype distribution is distorted in offspring of crossbred male heterozygous Smchd1^{MommeD1} mice and female hemizygous D4Z4-2.5 mice (tested at postnatal day 12). Statistical analysis was performed using Pearson's chi-squared test. P=0.0054. (**B**) Gender distribution is distorted in offspring of crossbred male heterozygous Smchd1^{MommeD1} mice and female hemizygous D4Z4-2.5 mice (tested at postnatal day 12). Statistical analysis was performed using Pearson's chi-squared test. P=0.0003. (**C**) The body weight of D4Z4-2.5/Smchd1^{MommeD1} mice is significantly reduced at postnatal day 15 compared with the body weight of littermates. Statistical analysis was performed using one-way ANOVA followed by Tukey post hoc test. ****$P<0.0001$. (**D**) The body weight of D4Z4-2.5/Smchd1^{MommeD1} mice from postnatal day 12 until postnatal day 22. Seven mice lost body weight so quickly that they had to be euthanized on postnatal day 15; fourteen mice retained their body weight or gained some body weight from 12 days until 22 days of age. Black circles represent male mice; grey circles represent female mice. Each circle represents a single mouse (C, D).

a heterozygous Smchd1^{MommeD1} mutation (D4Z4–2.5/Smchd1^{MommeD1} mice) compared with hemizygous D4Z4–2.5 mice without the Smchd1^{MommeD1} mutation (Fig. 1B). Sanger sequencing showed that only Smchd1 transcripts from the wild-type allele were present (data not shown). Thus, the mutant Smchd1 transcript seems to be rapidly degraded in concordance with a previous report (21). To determine the effect of the Smchd1^{MommeD1} mutation on the chromatin structure of the D4Z4 repeat, we measured DNA methylation at the region just distal to the D4Z4 repeat (25). We found significantly reduced DNA methylation levels at two CpG dinucleotides in DNA isolated from the tails of D4Z4–2.5/Smchd1^{MommeD1} mice compared with D4Z4–2.5 mice (Fig. 1C). We also detected a significantly lower chromatin compaction score (ChCS; H3K9me3 level, a repressive chromatin mark, corrected for H3K4me2 level, an active chromatin mark) (26) in D4Z4–2.5/Smchd1^{MommeD1} mice when we performed histone ChIP analysis using D4Z4-specific primers (9) in fibroblasts isolated from D4Z4–2.5 and D4Z4–2.5/Smchd1^{MommeD1} neonates (Fig. 1D; $P = 0.0108$). Previously, we have shown that the ChCS is significantly reduced in both fibroblasts and myoblasts of FSHD patients compared with control individuals (26), which is why we refrained from testing the ChCS in myoblasts of the mice. Our results suggested that the Smchd1^{MommeD1} mutation could potentially affect DUX4 transcript levels by modulating the

measured at the region immediately distal to the D4Z4 repeat array in tail DNA of six D4Z4-2.5 (M1-M6) and six D4Z4-2.5/Smchd1^{MommeD1} (M7-M12) mice (postnatal day 15). The bisulphite primers used amplify a region containing 10 CpG dinucleotides. Results are shown for 10 individual plasmid DNA samples per mouse. Open circles represent unmethylated CpG dinucleotides; closed circles represent methylated CpG dinucleotides. The bottom row shows the average DNA methylation level of each CpG dinucleotide per genotype. Statistical analysis was performed using Student's *t*-tests and multiple testing correction was performed by the Holm-Sidak method. *$P<0.05$. (**D**) Relative chromatin compaction score (ChCS; H3K9me3 level corrected for H3K4me2 level) of the D4Z4 transgene in fibroblasts isolated from neonatal D4Z4-2.5 and D4Z4-2.5/Smchd1^{MommeD1} mice (postnatal day 2). Statistical analysis was performed using Student's *t*-test.*$P<0.05$. (**E**) Relative DUX4 expression in myoblast and myotube cultures generated from the EDL muscle of D4Z4-2.5 and D4Z4-2.5/Smchd1^{MommeD1} mice (postnatal day 15). No statistical analysis was performed due to the low sample number. (**F**) Relative *Mef2c* expression (myogenic differentiation marker) in myoblast and myotube cultures generated from the EDL muscle of D4Z4-2.5 and D4Z4-2.5/Smchd1^{MommeD1} mice (postnatal day 15). MB = myoblast culture; MT = myotube culture; 2.5 = D4Z4-2.5 mouse; 2.5/S^{M} = D4Z4-2.5/Smchd1^{MommeD1} mouse. No statistical analysis was performed due to the low sample number. Each bar represents a single mouse; error bars represent standard deviations for technical replicates (A, B, D–F).

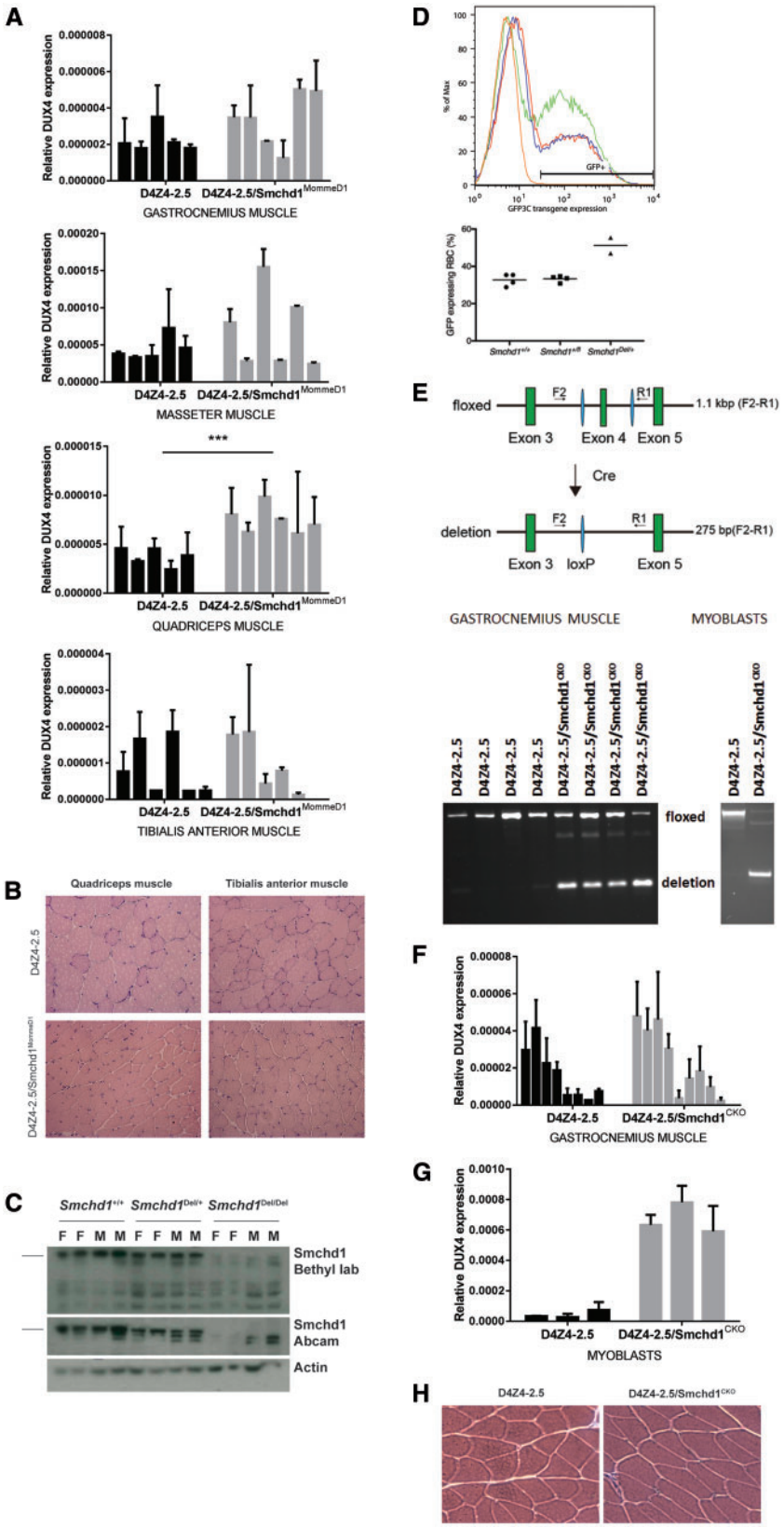

Figure 3. Skeletal muscles of the D4Z4–2.5 mouse are relatively insensitive to reduced Smchd1 levels. (**A**) Relative DUX4 expression in four different skeletal muscles of D4Z4-2.5 and D4Z4-2.5/Smchd1^{MommeD1} mice (postnatal day 15). Statistical analysis was performed on the average DUX4 expression in each mouse using Student's *t*-test (masseter muscle, quadriceps muscle) or Mann–Whitney *U* test (gastrocnemius muscle, TA muscle). ***$P<0.001$. (**B**) Representative H&E-stained cross sections (20× magnification) of quadriceps muscle and TA muscle of D4Z4-2.5 and D4Z4-2.5/Smchd1^{MommeD1} mice (postnatal day 15). (**C**) Western blot analysis of E12.5 embryo lysates of the given genotype and sex (F = female, M = male). The membrane was hybridised with two different Smchd1 antibodies, and compared with actin as a control. Smchd1 full-length protein is marked with a line. Smchd1$^{Del/Del}$ samples do not show detectable full-length Smchd1 with either Smchd1 antibody. (**D**) Expression

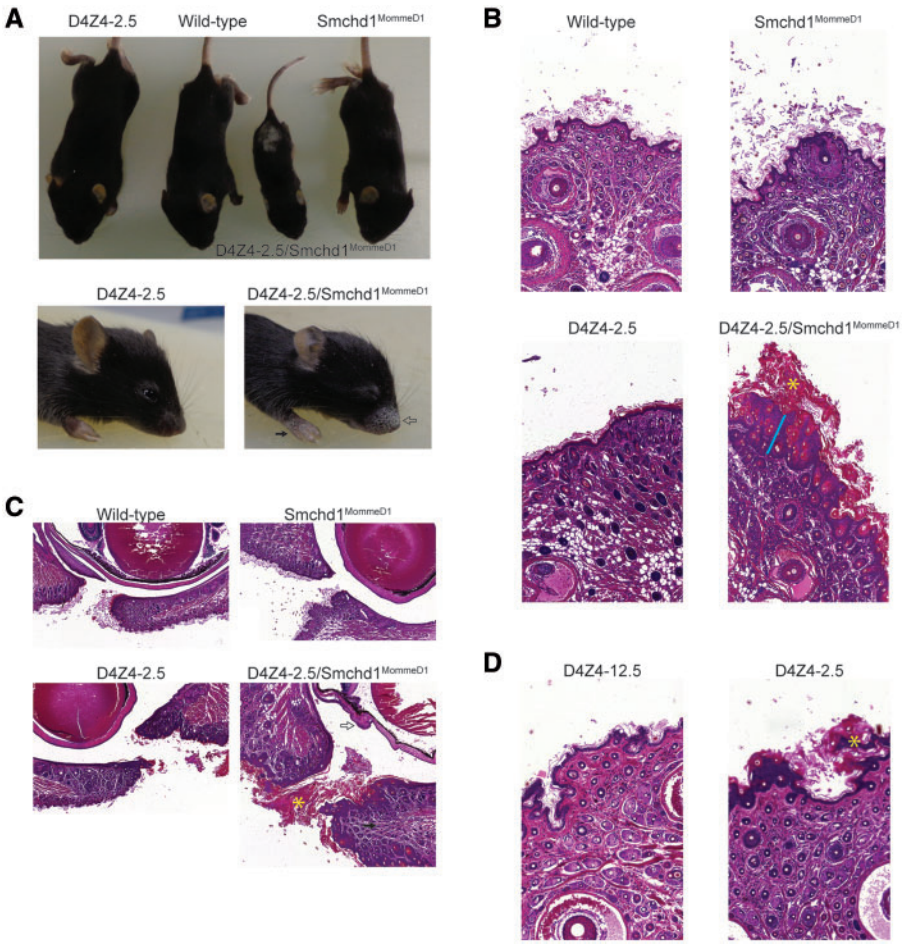

Figure 4. D4Z4–2.5/Smchd1^{MommeD1} mice develop skin hyperkeratosis and alopecia at young age, while D4Z4–2.5 mice present with a mild skin phenotype at 9 weeks of age. (**A**) Upper picture: A representative litter of pups born from crossbreeding a male heterozygous Smchd1^{MommeD1} mouse with a female hemizygous D4Z4-2.5 mouse (postnatal day 15). Lower picture: D4Z4-2.5/Smchd1^{MommeD1} mice show skin hyperkeratosis in the muzzle area (open arrow), on the eyelids, on the distal ends of the limbs (closed arrow), and focal alopecia in the distal dorsal part of the trunk starting from postnatal day 10. (**B**) Representative longitudinal sections of complete heads of the four different genotypes stained with H&E at postnatal day 15 (200× magnification of the skin around the muzzle). The muzzle skin features of D4Z4-2.5/Smchd1^{MommeD1} mice consist of extensive hyperkeratosis (asterisk), associated with thickening of the epidermis (blue line). (**C**) Representative longitudinal H&E stained sections of complete heads of the four different genotypes showing the eyelid area at postnatal day 15 (100× magnification). The eyelids of D4Z4-2.5/Smchd1^{MommeD1} mice show extensive hyperkeratosis (asterisk) with underlying keratitis (open arrow). The dermis shows an inflammatory infiltrate that is mostly composed of lymphocytes and a minority of macrophages (black arrow). (**D**) Representative longitudinal sections of complete heads of control D4Z4-12.5 mice and FSHD D4Z4-2.5 mice stained with H&E at 9 weeks of age (200× magnification of the skin around the muzzle). The muzzle skin phenotype of D4Z4-2.5 mice consists of mild hyperkeratosis (asterisk) that is visible from adulthood.

chromatin structure of the D4Z4 transgene. We therefore analysed DUX4 expression in a small set of myoblast cultures generated from the extensor digitorum longus (EDL) muscles of D4Z4–2.5 and D4Z4–2.5/Smchd1^{MommeD1} mice. DUX4 transcript levels were highly increased in myotube cultures that were differentiated for 48 h (differentiation was confirmed by measuring *Mef2c* expression), and slightly increased in proliferating myoblast cultures of D4Z4–2.5/Smchd1^{MommeD1} mice compared with D4Z4–2.5 mice (Fig. 1E and F). Thus, Smchd1 haploinsufficiency potentially affects DUX4 expression.

Genotype distribution, gender distribution, and body weight are distorted in mice born from D4Z4–2.5/Smchd1^{MommeD1} crossbreedings

Because of the known role of Smchd1 in X chromosome inactivation (21), each crossbreeding pair in our study consisted of a male Smchd1^{MommeD1} mouse and a female D4Z4–2.5 mouse, even though adult heterozygous Smchd1^{MommeD1} females present with normal *Hprt1* DNA methylation levels (20,21). To date, approximately 300 pups born from D4Z4–2.5/Smchd1^{MommeD1}

of the GFP3C transgene in 3-week-old mice hemizygous for the transgene, and Smchd1$^{+/+}$ (red line), Smchd1$^{+/fl}$ (blue line) or Smchd1$^{Del/+}$ (green line). Non-transgenic mice were used as controls (orange line). Upper picture: Representative flow cytometry profiles. Lower picture: Percentage of GFP-expressing erythrocytes for all mice tested. (**E**) Upper picture: Schematic of PCR analysis that was performed to detect floxed and deletion alleles in D4Z4-2.5/Smchd1^{CKO} mice. Lower picture: *Smchd1* deletion in gastrocnemius muscle and myoblast cultures of D4Z4-2.5/Smchd1^{CKO} mice. (**F**) Relative DUX4 expression in gastrocnemius muscle of D4Z4-2.5 and D4Z4-2.5/Smchd1^{CKO} mice. Statistical analysis was performed on the average DUX4 expression in each mouse using Student's *t*-test. (**G**) Relative DUX4 expression in myoblast cultures generated from the gastrocnemius muscle of D4Z4-2.5 and D4Z4-2.5/Smchd1^{CKO} mice. No statistical analysis was performed due to the low sample number. (**H**) Representative H&E-stained cross sections of gastrocnemius muscle of D4Z4-2.5 and D4Z4-2.5/Smchd1^{CKO} mice (32× magnification). Each bar represents a single mouse; error bars represent standard deviations for technical replicates (A, F, G).

crossbreedings have been genotyped. We found that at postnatal day 12 the genotype distribution of the pups that were born from these crossbreedings was significantly distorted (Fig. 2A; $P = 0.0054$). This is probably because fewer D4Z4–2.5/Smchd1^{MommeD1} mice were born, but more pups need to be genotyped to statistically confirm this hypothesis. In addition, less female mice were present at postnatal day 12 (Fig. 2B; $P = 0.0003$). We furthermore observed that during the first days after birth the D4Z4–2.5/Smchd1^{MommeD1} mice gained weight and were able to feed, as evidenced by stomachs filled with milk. However, D4Z4–2.5/Smchd1^{MommeD1} mice, both males and females, presented with a runting phenotype; the mice were smaller and exhibited an approximate 25% reduction in body weight compared with their littermates at postnatal day 15, although there was considerable variation in body weight reduction (Fig. 2C; $P < 0.0001$). We followed a cohort of 21 D4Z4–2.5/Smchd1^{MommeD1} mice from postnatal day 12 and found that 7 D4Z4–2.5/Smchd1^{MommeD1} mice (all males) quickly lost body weight. These mice were therefore euthanized at postnatal day 15. In contrast, the other 14 D4Z4–2.5/Smchd1^{MommeD1} mice (10 males and 4 females) retained or gained body weight from 12 days until 22 days of age (Fig. 2D). Due to the large difference in body weight compared with littermates with other genotypes, all remaining D4Z4–2.5/Smchd1^{MommeD1} mice were euthanized at postnatal day 22. In conclusion, a non-Mendelian inheritance pattern is observed for the pups born from D4Z4–2.5/Smchd1^{MommeD1} crossbreedings, and D4Z4–2.5/Smchd1^{MommeD1} mice are runted.

Skeletal muscles of the D4Z4–2.5 mouse are relatively insensitive to reduced Smchd1 levels

We previously reported low and variable DUX4 expression in skeletal muscles of D4Z4–2.5 mice (15). To determine whether Smchd1 has a modifier role by regulating DUX4 expression *in vivo*, we quantified DUX4 transcript levels in four different skeletal muscles of D4Z4–2.5 and D4Z4–2.5/Smchd1^{MommeD1} mice [gastrocnemius muscle, masseter muscle, quadriceps muscle, and tibialis anterior (TA) muscle]. DUX4 expression was significantly increased in only one of the tested muscles of the D4Z4–2.5/Smchd1^{MommeD1} mice compared with the D4Z4–2.5 mice, namely only in the quadriceps muscle (Fig. 3A; $P = 0.0006$). In addition to the very low DUX4 transcript levels (Cq values varied between 30 and 35), a possible explanation for this observation may be the prominent interindividual variability in DUX4 expression that we observed. In addition, the skeletal muscles of D4Z4–2.5/Smchd1^{MommeD1} mice did not show overt skeletal muscle pathology, as tested by haematoxylin and eosin (H&E) staining of the quadriceps muscle and the TA muscle (Fig. 3B). Therefore, we hypothesized that skeletal muscles of the D4Z4–2.5 mouse are relatively insensitive to reduced Smchd1 levels.

To further address this hypothesis, we studied the D4Z4–2.5/Smchd1^{CKO} mouse model. This mouse model was generated by crossbreeding the D4Z4–2.5 mouse model with mice that carry exon 4 of *Smchd1* floxed (Smchd1$^{fl/fl}$ mice) and express Cre recombinase from the muscle-specific promoter Myf5 (27). Smchd1$^{fl/fl}$ mice are viable and fertile, suggesting that the allele is not hypomorphic. From heterozygous intercrosses between Smchd1$^{Del/+}$ mice [produced by crossbreeding Smchd1$^{fl/fl}$ mice with a constitutive CMV-driven Cre recombinase mouse strain (28)], no Smchd1$^{Del/Del}$ mice were observed at weaning (99 pups were tested). This is consistent with the expected embryonic lethality of a null allele on the C57BL/6 background (21). Both male ($n = 8$) and female ($n = 5$) Smchd1$^{Del/Del}$ embryos were observed at E12.5 and loss of the Smchd1 protein in these embryos was confirmed by Smchd1 western blot (Fig. 3C). However, all females were very small, consistent with mid-gestation lethality as observed for other *Smchd1* null alleles (21). As Smchd1 was first identified using a multicopy GFP transgene array, directed to express in red blood cells (20,21), we also tested the effect of the floxed and deleted alleles on the expression of the GFP3C transgene. We found no changes in expression with the floxed allele, but an increased expression in Smchd1$^{Del/+}$ mice (Fig. 3D), confirming that the floxed allele behaves as a wild-type allele and the deleted allele as a null allele.

In the D4Z4–2.5/Smchd1^{CKO} mice we tested, the *Smchd1* gene was disrupted on both alleles in Myf5-positive cells (Fig. 3E). DUX4 transcript levels were not significantly increased in the complete gastrocnemius muscle (Fig. 3F), but we did measure increased DUX4 expression in muscle cultures generated from the gastrocnemius muscle (Fig. 3G), which is in line with our results obtained in D4Z4–2.5/Smchd1^{MommeD1} mice. Furthermore, D4Z4–2.5/Smchd1^{CKO} mice presented with no additional phenotypes compared with D4Z4–2.5 mice; also no muscular dystrophy phenotype was detected by H&E staining (Fig. 3H). Together, these data indeed suggest that skeletal muscles of the D4Z4–2.5 mouse are largely unaffected by reduced Smchd1 levels.

D4Z4–2.5/Smchd1^{MommeD1} mice develop skin hyperkeratosis and alopecia at young age, while D4Z4–2.5 mice present with a mild skin phenotype at 9 weeks of age

Besides the runting phenotype, D4Z4–2.5/Smchd1^{MommeD1} mice developed alopecic and hyperkeratotic areas around the nose (muzzle skin), on the dorsal aspect of all paws, and in approximately 10% of cases on the upper back of the trunk region, starting at 10 days of age (Fig. 4A). The hyperkeratotic skin had a scaly appearance. The skin lesions appeared in all mice and no gender differences were observed. In addition, between postnatal days 11 and 14, when littermates started to open their eyes, the D4Z4–2.5/Smchd1^{MommeD1} mice had difficulties opening their eyes (Fig. 4A). Similar to the skin phenotype, the penetrance of this phenotype was 100% and not gender-dependent. To gain more insight into these phenotypes, we performed histopathological examination of the mice at postnatal day 15. Serial sections of complete heads of the D4Z4–2.5/Smchd1^{MommeD1} mice ($n = 3$) revealed, particularly in the areas around the muzzle and the eyelids, thickening of the stratum corneum with increased layers of keratin (orthokeratotic and parakeratotic hyperkeratosis), thickening of the epidermis reaching 8–10 layers (epidermal hyperplasia) with irregular rete ridges formations (downward projections of the epidermis) (Fig. 4B), and minimal lymphocytic inflammation in the dermis (Fig. 4C). In contrast, histopathological investigation of the complete heads of juvenile wild-type mice ($n = 3$), Smchd1^{MommeD1} mice ($n = 3$), and D4Z4–2.5 mice ($n = 3$) was normal with no skin lesions apparent at 15 days of age (Fig. 4B and C). Gross and histological examination of all organs revealed no abnormalities for all four genotypes tested at postnatal day 15 (data not shown).

As shown previously, approximately 50% of D4Z4–2.5 mice develop eye abnormalities, possibly due to incomplete closure of the eyelids. The typical onset of the eye phenotype in D4Z4–2.5 mice is around 8–12 weeks of age (15). In our current study, histopathological examination did not reveal skin abnormalities that could explain these eye abnormalities in D4Z4–2.5 mice at postnatal day 15. To test whether D4Z4–2.5 mice develop a skin

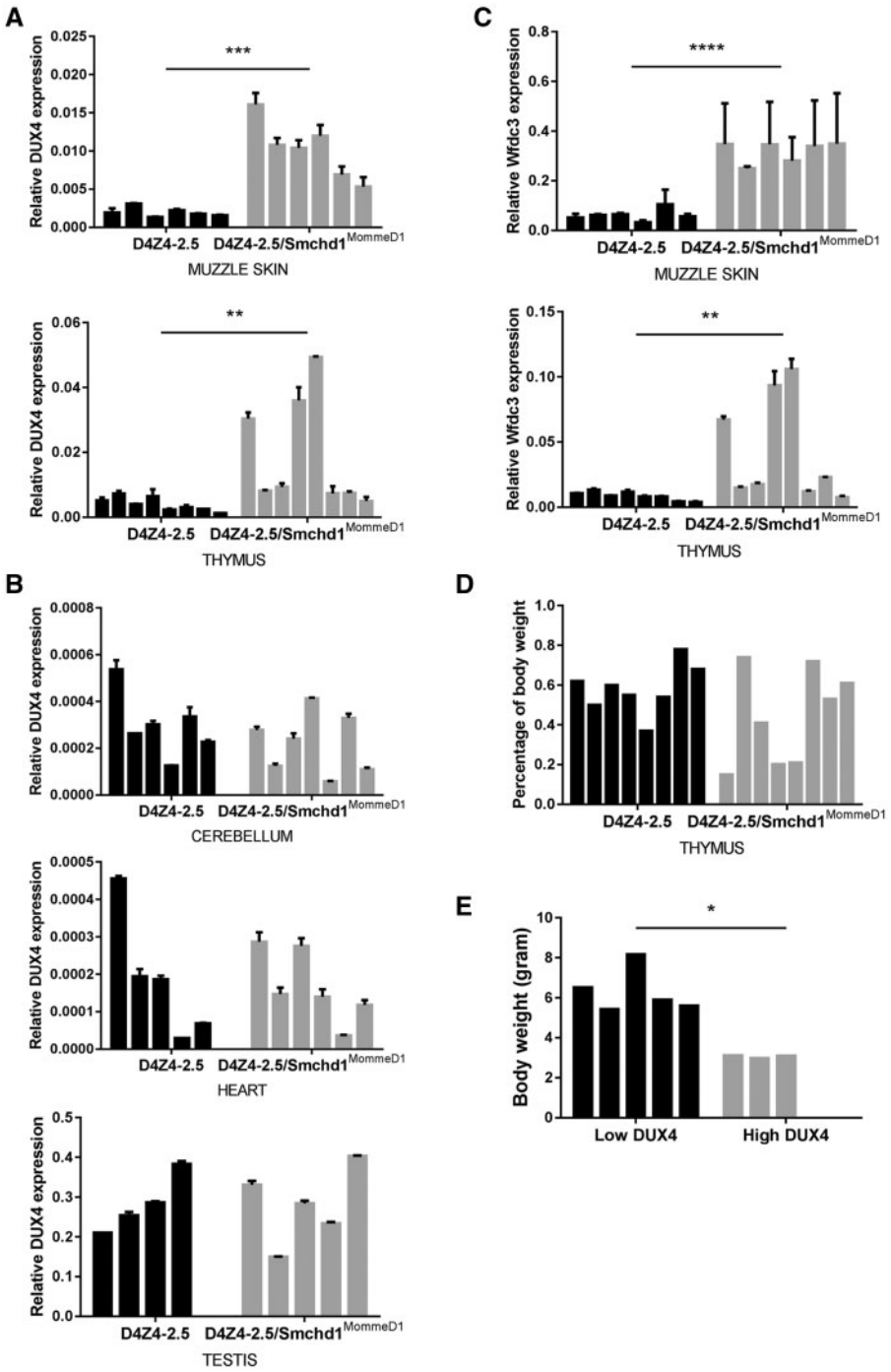

Figure 5. Skin and thymus of the D4Z4–2.5 mouse are sensitive to Smchd1 haploinsufficiency. (**A**) Relative DUX4 expression in muzzle skin and thymus of D4Z4-2.5 and D4Z4-2.5/Smchd1^{MommeD1} mice (postnatal day 15). Statistical analysis was performed on the average DUX4 expression in each mouse using Student's *t*-test (muzzle skin) or Mann–Whitney *U* test (thymus). $^{**}P<0.01$; $^{***}P<0.001$. (**B**) Relative DUX4 expression in cerebellum, heart, and testis of D4Z4-2.5 and D4Z4-2.5/Smchd1^{MommeD1} mice (postnatal day 15). Statistical analysis was performed on the average DUX4 expression in each mouse by Student's *t*-test. (**C**) Relative *Wfdc3* expression in muzzle skin and thymus of D4Z4-2.5 and D4Z4-2.5/Smchd1^{MommeD1} mice (postnatal day 15). Statistical analysis was performed on the average *Wfdc3* expression in each mouse using Student's *t*-test (muzzle skin) or Mann–Whitney *U* test (thymus). $^{**}P<0.01$; $^{****}P<0.0001$. (**D**) Thymus weight (depicted as percentage of total body weight) of D4Z4-2.5 and D4Z4-2.5/Smchd1^{MommeD1} mice (postnatal day 15). Statistical analysis was performed using Student's *t*-test. The order of results is similar as in Figure 5A, thus showing an inverse relationship between DUX4 expression and thymus weight. (**E**) Body weight of D4Z4-2.5/Smchd1^{MommeD1} mice at postnatal day 15. The mice are divided into two groups; group 1 consisted of 5 mice that presented with relatively low DUX4 transcript levels in the thymus, while group 2 consisted of 3 mice with very high DUX4 expression in the thymus. Statistical analysis was performed using Mann–Whitney *U* test. $^{*}P<0.05$. Each bar represents a single mouse; error bars represent standard deviations for technical replicates.

Table 1. High DUX4 expression in the thymus of D4Z4–2.5/Smchd1^{MommeD1} mice does not disturb intrathymic development of thymocytes. CD4 T cells and CD8 T cells develop in the thymus from bone marrow progenitors. In short, immature thymocyte progenitors [CD4/CD8 double-negative (DN) cells] differentiate into CD4/CD8 double-positive (DP) cells to produce CD4 single-positive T cells or CD8 single-positive T cells. To expand into the DP population, DN cells first undergo a developmental process consisting of 4 stages: DN1, DN2, DN3, and DN4 (29). Average percentage of specific cell populations (± standard deviation of biological replicates) in the thymus is shown for five wild-type (WT) mice and four D4Z4–2.5/Smchd1^{MommeD1} mice. The percentage of DN cells, DP cells, CD4 cells, and CD8 cells is obtained from the total number of cells in the thymus. The percentage of DN1 cells, DN2 cells, DN3 cells, and DN4 cells is obtained from the number of DN cells in the thymus. Statistical analysis was performed using two-way ANOVA followed by Holm-Sidak multiple comparison tests; the ratio of DN: DP: CD4: CD8 was compared between wild-type mice and D4Z4–2.5/Smchd1^{MommeD1} mice in one analysis, the ratio of DN1: DN2: DN3: DN4 was compared between wild-type mice and D4Z4–2.5/Smchd1^{MommeD1} mice in a second analysis.

Cell population	Flow cytometry markers	WT (% of cells)	D4Z4–2.5/Smchd1^{MommeD1} (% of cells)
DN	CD4(−)/CD8(−)	3.96 ± 1.67	3.51 ± 0.62
DP	CD4(+)/CD8(+)	82.76 ± 6.33	82.55 ± 3.70
CD4	CD4(+)/CD8(-)	8.11 ± 0.78	7.96 ± 0.77
CD8	CD4(−)/CD8(+)	1.86 ± 0.44	1.90 ± 0.46
DN1	CD4(−)/CD8(−)/CD25(−)/CD44(+)	14.70 ± 3.35	15.38 ± 0.78
DN2	CD4(−)/CD8(−)/CD25(+)/CD44(+)	10.90 ± 4.03	11.68 ± 3.19
DN3	CD4(−)/CD8(−)/CD25(+)/CD44(−)	17.87 ± 11.59	12.87 ± 7.95
DN4	CD4(−)/CD8(−)/CD25(−)/CD44(−)	56.56 ± 17.93	60.10 ± 11.52

phenotype in adulthood, we performed an additional histopathological examination of complete heads at 9 weeks of age and compared control D4Z4–12.5 mice ($n = 3$) with D4Z4–2.5 mice ($n = 3$). A mild skin phenotype consisting of hyperkeratosis was indeed observed around the muzzle and the eyelids of D4Z4–2.5 mice, while no skin pathology was observed in the D4Z4–12.5 mice (Fig. 4D). Thus, D4Z4–2.5 mice, like D4Z4–2.5/Smchd1^{MommeD1} mice, present with eye and skin phenotypes. However, these phenotypes develop earlier and are more severe in D4Z4–2.5/Smchd1^{MommeD1} mice, as is expected from the hypothesized modifier role of Smchd1 at the D4Z4 repeat array.

Skin and thymus of the D4Z4–2.5 mouse are sensitive to Smchd1 haploinsufficiency

The phenotype of D4Z4–2.5/Smchd1^{MommeD1} mice seems restricted to the body weight and the skin, with consequences for the eyes. We therefore hypothesized that skin tissue is more sensitive to Smchd1 haploinsufficiency and presents with higher DUX4 transcript levels than skeletal muscles and other non-skeletal muscle tissues. To test our hypothesis, we measured DUX4 transcript levels in muzzle skin and in additional non-skeletal muscle tissues, namely brain (cerebellum), heart, testis, and thymus. Indeed, DUX4 expression was significantly increased in the muzzle skin of D4Z4–2.5/Smchd1^{MommeD1} mice compared with D4Z4–2.5 mice (Fig. 5A; $P = 0.0004$), whereas DUX4 transcript levels in the cerebellum, heart, and testis were unchanged (Fig. 5B). Unexpectedly, DUX4 expression was also significantly increased in the thymus of D4Z4–2.5/Smchd1^{MommeD1} mice (Fig. 5A; $P = 0.0011$). We also tested the expression of the DUX4 target gene *Wfdc3* (15) in muzzle skin and thymus, and observed a significant increase in *Wfdc3* transcript levels in both tissues of D4Z4–2.5/Smchd1^{MommeD1} mice (Fig. 5C; $P < 0.01$). Interestingly, DUX4 expression in the thymus of D4Z4–2.5/Smchd1^{MommeD1} mice was highly variable. Of the eight mice tested, only three D4Z4–2.5/Smchd1^{MommeD1} mice showed increased DUX4 expression in the thymus compared with D4Z4–2.5 mice. We found an inverse relationship between the thymus weight and DUX4 expression in the thymus; the D4Z4–2.5/Smchd1^{MommeD1} mice with the lowest thymus weight presented with the highest DUX4 transcript levels (Fig. 5A and D). We also observed that the body weight of the D4Z4–2.5/Smchd1^{MommeD1} mice with the highest DUX4 expression in the thymus was significantly reduced compared with D4Z4–2.5/Smchd1^{MommeD1} mice with lower DUX4 transcript levels in the thymus (Fig. 5E; $P = 0.0357$). In conclusion, our data indicate that, in contrast to the skeletal muscles and some non-skeletal muscle tissues, skin and thymus are highly affected by Smchd1 haploinsufficiency.

High DUX4 expression in the thymus of D4Z4–2.5/Smchd1^{MommeD1} mice does not disturb intrathymic T cell development

We found high DUX4 transcript levels in the thymus of D4Z4–2.5/Smchd1^{MommeD1} mice (average Cq value of 22) and an inverse relationship between DUX4 expression in the thymus and body weight. Therefore, we hypothesized that the runting phenotype observed in D4Z4–2.5/Smchd1^{MommeD1} mice is linked to increased DUX4 expression in the thymus. Interestingly, mouse Duxbl (also known as Duxl), whose homeodomains show 67% identity to those of DUX4, was identified as a transcription factor with a critical role in the development of CD4/CD8 double-negative (DN) mouse thymocytes (29–30). Normal expression levels of Duxbl in the thymus stimulate the switch from CD44^{high}/CD25^{+} DN thymocytes to CD44^{low}/CD25^{+} DN thymocytes, while constitutive Duxbl expression disturbs the production of CD4/CD8 double-positive (DP) thymocytes (29). We performed flow cytometry analysis of the thymuses of wild-type mice and D4Z4–2.5/Smchd1^{MommeD1} mice at postnatal day 15 to determine the percentage of DN thymocytes (subdivided into DN1-DN4 thymocytes), DP thymyocytes, and single CD4 thymocytes and single CD8 thymocytes. Although the total number of thymocytes in the D4Z4–2.5/Smchd1^{MommeD1} mice was significantly reduced (data not shown), which was not surprising because of the reduced thymus weight in some D4Z4–2.5/Smchd1^{MommeD1} mice, the percentage of DN1, DN2, DN3, and DN4 thymocytes and the percentage of DN, DP, CD4, and CD8 thymocytes was not changed between wild-type mice and D4Z4–2.5/Smchd1^{MommeD1} mice (Table 1). In addition, gross and histological examination of the thymus of D4Z4–2.5/Smchd1^{MommeD1} mice at postnatal day 15 appeared normal (data not shown). Our data suggest that the development of thymocytes in D4Z4–2.5/Smchd1^{MommeD1} mice is not blocked and that it is unlikely that DUX4 interferes with Duxbl function as an explanation for the thymus pathology.

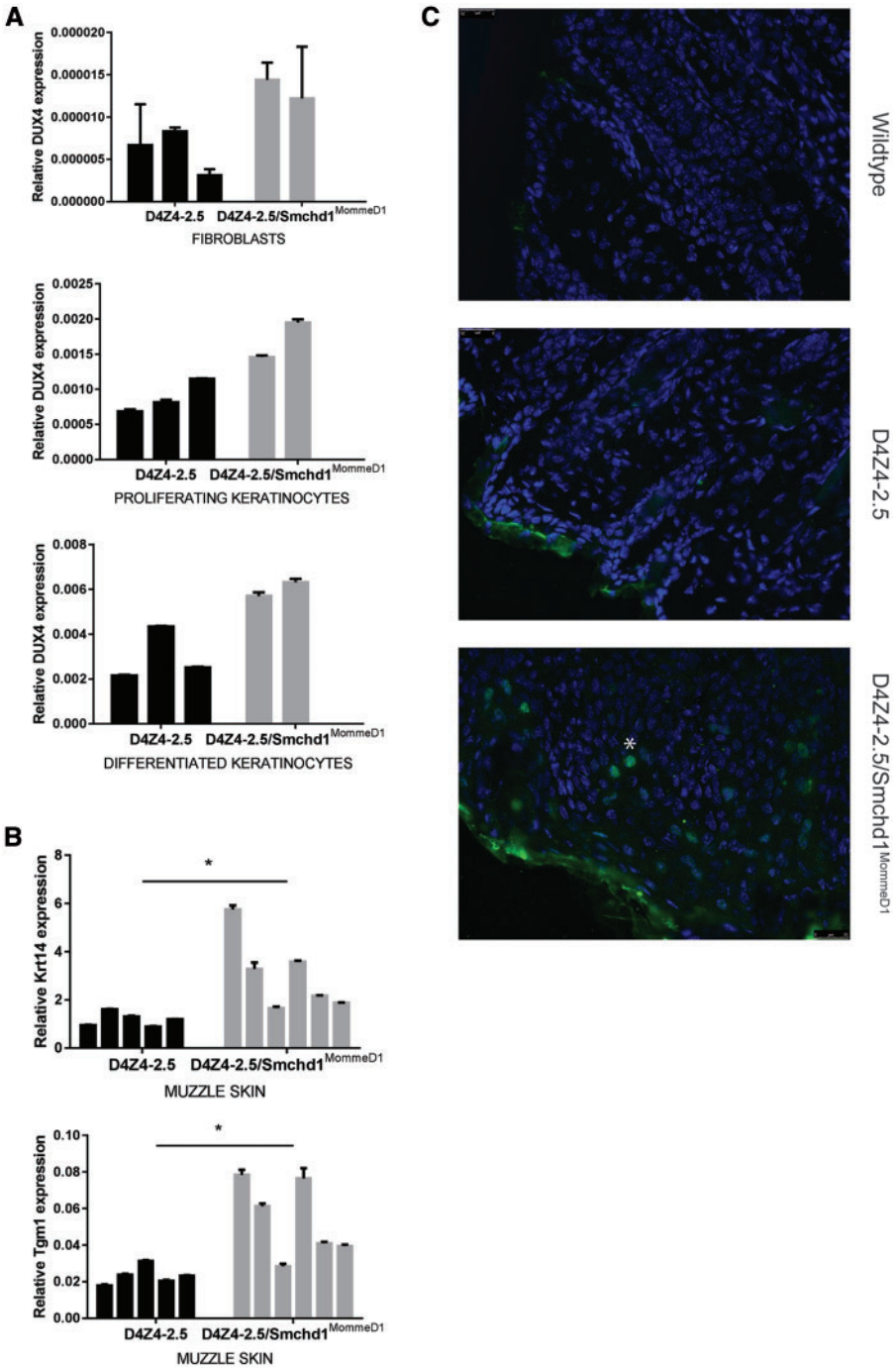

Figure 6. DUX4 is highly expressed in keratinocytes of D4Z4–2.5/Smchd1^{MommeD1} mice. (**A**) Relative DUX4 expression in fibroblasts, proliferating keratinocytes, and keratinocytes that were differentiated for 7 days generated from skin of D4Z4-2.5 and D4Z4-2.5/Smchd1^{MommeD1} mice. No statistical analysis was performed due to low sample number. (**B**) Relative keratin 14 (Krt14) and transglutaminase 1 (Tgm1) expression in the muzzle skin of D4Z4-2.5 and D4Z4-2.5/Smchd1^{MommeD1} mice. Statistical analysis was performed on the average expression in each mouse using Student's *t*-test (Tgm1) or Mann–Whitney *U* test (Krt14). *$P<0.05$. (**C**) Representative longitudinal sections of the muzzle skin of wild-type, D4Z4-2.5, and D4Z4-2.5/Smchd1^{MommeD1} mice stained with DAPI and DUX4 at postnatal day 15 (20x magnification). An example of a DUX4-positive cell in the epidermal cell layer of the muzzle skin of a D4Z4-2.5/Smchd1^{MommeD1} mouse is marked with an asterisk. Each bar represents a single mouse; error bars represent standard deviations for technical replicates (A, B).

DUX4 is highly expressed in keratinocytes

To determine what cell type in muzzle skin expresses DUX4, we isolated total skin from D4Z4–2.5 and D4Z4–2.5/Smchd1^{MommeD1} neonates and separated dermis and epidermis to isolate fibroblasts and keratinocytes, respectively. Interestingly, DUX4 transcript levels were very high in keratinocytes (Cq values around 26 in proliferating keratinocytes; Cq values around 24 in keratinocytes that were differentiated for 7 days), while DUX4 expression in fibroblasts was low (Cq values around 33). We also observed higher DUX4 transcript levels in fibroblasts,

proliferating keratinocytes, and differentiated keratinocytes of D4Z4–2.5/Smchd1^{MommeD1} mice compared with D4Z4–2.5 mice (Fig. 6A). We next tested the transcript levels of two keratinocyte differentiation markers, keratin 14 (Krt14) and transglutaminase 1 (Tgm1), in the muzzle skin of D4Z4–2.5 and D4Z4–2.5/Smchd1^{MommeD1} mice. We detected increased transcript levels for both markers in the muzzle skin of D4Z4–2.5/Smchd1^{MommeD1} mice compared with D4Z4–2.5 mice (Fig. 6B; $P < 0.05$). Finally, we tested DUX4 protein in the muzzle skin of the mice by immunofluorescence staining of muzzle skin sections. So far, we and others have not been able to detect DUX4 protein in tissues of the D4Z4–2.5 mouse. This is most likely due to low DUX4 transcript levels in combination with the lack of a sensitive assay to detect DUX4 protein. Only after isolating muscle fibres from the EDL muscle and generating myotube cultures, DUX4 protein could be detected in sporadic muscle nuclei (15). As DUX4 transcript levels are high in the muzzle skin of D4Z4–2.5/Smchd1^{MommeD1} mice, we expected that we could detect DUX4 protein by immunofluorescence staining. Indeed, we found that the epidermal cell layer of muzzle skin, mainly consisting of keratinocytes, of D4Z4–2.5/Smchd1^{MommeD1} mice expresses DUX4 protein (Fig. 6C). In contrast, we did not detect appreciable DUX4 protein in muzzle skin of wild-type and D4Z4–2.5 mice, even though DUX4 transcript levels were also relatively high in the muzzle skin of D4Z4–2.5 mice. Our results suggest that high DUX4 expression in combination with reduced Smchd1 levels in the skin may affect the keratinization process in mice.

Discussion

Previously, we described the D4Z4–2.5 mouse model that carries an FSHD-sized D4Z4 repeat array of 2.5 units. Although these transgenic mice can be used to study the *in vivo* epigenetic regulation of the D4Z4 repeat array locus, the expression of DUX4 in skeletal muscles is low and no muscular dystrophy phenotype has been observed (15). Interestingly, variants in *SMCHD1* have not only been identified in FSHD2 patients, but also in FSHD1 patients. FSHD patients with both a contracted D4Z4 repeat array and a *SMCHD1* mutation present with an unusually high clinical severity and potentially higher DUX4 transcript levels in skeletal muscles as suggested by SMCHD1 knockdown experiments in FSHD1 myotube cultures (13). By crossbreeding hemizygous D4Z4–2.5 female mice with heterozygous Smchd1^{MommeD1} male mice (20), we expected to detect increased DUX4 expression in skeletal muscles of D4Z4–2.5/Smchd1^{MommeD1} mice, and possibly muscle pathology.

The analysis of *Smchd1* transcript levels in a diverse set of tissues revealed reduced *Smchd1* expression in mice carrying the Smchd1^{MommeD1} mutation. In addition, we found reduced DNA methylation levels in the region immediately distal to the D4Z4 repeat array and a more open chromatin structure at the D4Z4 repeat array, as measured by the chromatin compaction score (H3K9me3 level corrected for H3K4me2 level). However, only two CpG dinucleotides in the region distal to the D4Z4 repeat array (25) were differentially methylated between D4Z4–2.5 and D4Z4–2.5/Smchd1^{MommeD1} mice. It will be interesting to determine why specific CpG dinucleotides seem more sensitive to the presence of the Smchd1^{MommeD1} mutation. This may provide insight in the epigenetic regulation of the D4Z4 repeat array locus by SMCHD1, as it is currently unknown how SMCHD1 exactly affects the chromatin structure of the D4Z4 repeat array. The advantage of using the D4Z4–2.5 and D4Z4–2.5/Smchd1^{MommeD1} mouse models for such studies is that the mouse genome, unlike the human genome, does not contain D4Z4-like repeat units scattered throughout the genome. Furthermore, our data show that the epigenetic regulation of the D4Z4 transgene in D4Z4–2.5 and D4Z4–2.5/Smchd1^{MommeD1} mice parallels the epigenetic regulation observed in humans (15).

We observed that the genotype distribution was distorted on postnatal day 12 when crossbreeding a male heterozygous Smchd1^{MommeD1} mouse with a female hemizygous D4Z4–2.5 mouse. Our data suggest that fewer D4Z4–2.5/Smchd1^{MommeD1} are born from such crossbreedings. However, additional pups need to be genotyped to confirm this observation. We did not genotype pups before postnatal day 12 as we did not want to disturb the nest. Therefore, some D4Z4–2.5/Smchd1^{MommeD1} pups may have died between birth and 12 days of age, although we did not often observe dead pups in the cages. Alternatively, D4Z4–2.5/Smchd1^{MommeD1} mice may have died during embryogenesis, and this is currently under study. It will be interesting to analyse offspring from reciprocal crosses, since Smchd1 has a role in X chromosome inactivation (21).

The analysis of DUX4 transcript levels in a set of skeletal muscles, and in myoblast and myotube cultures generated from the EDL muscle, showed us that DUX4 expression is potentially increased in skeletal muscles of D4Z4–2.5/Smchd1^{MommeD1} mice compared with D4Z4–2.5 mice. However, DUX4 transcript levels in skeletal muscles of D4Z4–2.5/Smchd1^{MommeD1} mice were very low and we observed high interindividual variability in DUX4 expression. Furthermore, we did not observe muscle pathology in skeletal muscles of D4Z4–2.5/Smchd1^{MommeD1} mice nor in skeletal muscles of D4Z4–2.5/Smchd1^{CKO} mice. Therefore, we believe that skeletal muscles of D4Z4–2.5 mice are relatively insensitive to reduced Smchd1 levels. Alternatively, high DUX4 RNA and protein expression may only be measured in this mouse model during skeletal muscle regeneration. We recently showed that intramuscular cardiotoxin injections resulting in severe muscle damage and skeletal muscle regeneration were associated with significantly transient increased DUX4 transcript levels in the D4Z4–2.5 mouse model during early muscle regeneration (31). Due to the severe phenotype of D4Z4–2.5/Smchd1^{MommeD1} mice, we have refrained from performing similar experiments in these mice. However, it would be interesting to determine how Smchd1 haploinsufficiency affects DUX4 expression during *in vivo* skeletal muscle regeneration. Finally, our previous studies showed that DUX4 protein expression in D4Z4–2.5 mice is restricted to Myog-negative myoblasts; these cells do not fuse into myotubes (15). This contrasts with DUX4 protein expression in human myoblasts where DUX4-positive cells are typically myosin-positive and thus part of fused myotubes (18,19). A mouse model with DUX4 protein expression in myosin-positive cells may thus respond differently to Smchd1 haploinsufficiency in skeletal muscles, and may serve as a better model to study the modifier role of Smchd1 in the muscle phenotype. For example, a novel mouse model with muscle-specific doxycycline-regulated DUX4 expression that was recently generated presents with DUX4-positive nuclei surrounded by myosin heavy chain-positive cytoplasm (17). Unfortunately, this mouse model lacks a D4Z4 repeat array to which Smchd1 can bind and thus cannot be used to study Smchd1 haploinsufficiency in skeletal muscles.

In contrast to what we observed in skeletal muscles, Smchd1 haploinsufficiency impacts the skin and thymus of D4Z4–2.5 mice. We detected increased DUX4 transcript levels in muzzle skin and primary fibroblasts and keratinocytes isolated from D4Z4–2.5/Smchd1^{MommeD1} mice. In addition, D4Z4–2.5/Smchd1^{MommeD1} mice presented with a severe skin phenotype

starting from postnatal day 10, especially around the muzzle and on the paws. The eyelids were also affected as shown by histopathological examination and D4Z4–2.5/Smchd1^{MommeD1} mice had difficulties opening their eyes. These data give us the opportunity to explain the uncharacterized eye phenotype that was previously described for D4Z4–2.5 mice (15), since a similar, albeit milder, skin phenotype was detected in D4Z4–2.5 mice at 9 weeks of age. Furthermore, we detected increased DUX4 expression in the thymus of D4Z4–2.5/Smchd1^{MommeD1} mice. Interestingly, not all D4Z4–2.5/Smchd1^{MommeD1} mice presented with higher thymic DUX4 transcript levels than D4Z4–2.5 mice, and we identified an inverse relationship between DUX4 expression in the thymus and body weight. In addition, the D4Z4–2.5/Smchd1^{MommeD1} mice with very high thymic DUX4 transcript levels lost body weight so rapidly from postnatal day 12 that they had to be euthanized on postnatal day 15, while the body weight of the D4Z4–2.5/Smchd1^{MommeD1} mice with lower DUX4 expression in the thymus was still increasing at postnatal day 15. It is interesting that D4Z4–2.5/Smchd1^{MommeD1} mice show skin and runting phenotypes, as this is not the first DUX4 expressing mouse model with these phenotypes. A mouse model carrying a doxycycline-inducible transgene that encodes DUX4 and 3' genomic DNA, integrated into the mouse X chromosome, displays a variety of phenotypes including increased epidermal thickness and nuclear density in the dermis, and reduced body weight (24). In addition, a recent study of these iDUX4(2.7) mice showed that females are hyperactive and have significantly impaired hearing loss at high frequencies, while males show periods of increased respiration and catatonic torpor (32). We have not yet investigated these non-skeletal muscle phenotypes in D4Z4–2.5/Smchd1^{MommeD1} mice, but it may be worthwhile to study this in more detail because of the overlap in skin and runting phenotypes between the iDUX4(2.7) mouse model and the D4Z4–2.5/Smchd1^{MommeD1} mouse model. Overall, we conclude that haploinsufficiency for Smchd1 exacerbates the phenotype of the D4Z4–2.5 mouse model. However, the phenotype of D4Z4–2.5/Smchd1^{MommeD1} mice is still restricted to specific tissues, as was already observed in the D4Z4–2.5 mouse (15).

This study shows that Smchd1 haploinsufficiency aggravates the phenotype of the D4Z4–2.5 mouse model, a transgenic mouse model for FSHD1. Notably, our data reveal that the skin and the thymus of this mouse model are very sensitive to reduced Smchd1 levels, while skeletal muscles seem unaffected. To study muscle pathology associated with FSHD, other mouse models will need to be studied, such as the recently generated mouse model with muscle-specific doxycycline-regulated DUX4 expression (17). However, our study provides support that the D4Z4–2.5 mouse model can be used to study the epigenetic regulation of the D4Z4 repeat array. In addition, the D4Z4–2.5/Smchd1^{MommeD1} mouse model may be ideal to study the function of DUX4 in the epidermis and the thymus. Interestingly, DUX4 expression was recently reported in human skin and confluent keratinocytes. ChIP sequencing analysis showed that repressive H3K9me3 levels at the D4Z4 repeat array, both at chromosome 4q35 and chromosome 10q26, dropped significantly during confluence-induced squamous differentiation. Western blot analysis and immunohistochemistry detected DUX4 protein in keratinocytes in the epidermis of a control individual, and the full-length DUX4 transcript was also detected in confluent keratinocytes (33). Another study reported DUX4 expression, together with expression of the DUX4 target genes *TRIM43* and *MBD3L2*, in human thymus (34). In conclusion, DUX4 may have a function outside the germline.

Materials and Methods

D4Z4–2.5/Smchd1^{MommeD1} mice

D4Z4–2.5 mice and Smchd1^{MommeD1} mice were generated previously (15,20). All D4Z4–2.5/Smchd1^{MommeD1} mice were obtained by crossbreeding a male heterozygous Smchd1^{MommeD1} mouse with a female hemizygous D4Z4–2.5 mouse. Resulting offspring were genotyped by PCR analysis using tail DNA. The D4Z4–2.5 transgene was detected by PCR using the following primers: 5'-TGGTCCGTGAAGACATGTGT-3' and 5'- GAGCCCTCAGAGAAGT GGG-3'. The Smchd1^{MommeD1} mutation was detected by PCR with the following primers: 5'-CAATAGGTCCCCCTCATCAA-3' and 5'-CAGTGGCCAACCACATAACA-3'. An internal probe with the sequence 5'-CAACATAACAGCACAACCAAAGCTG-3' was added to the PCR mixture so that after the reaction the PCR product could be melted by Lightscanner (Idaho Technology Inc., Salt Lake City, USA) resulting in different melt curves for alleles with the Smchd1^{MommeD1} mutation and for alleles without the Smchd1^{MommeD1} mutation. Wild-type mice, Smchd1^{MommeD1} mice, and D4Z4–2.5 mice of the same genetic background as the D4Z4–2.5/Smchd1^{MommeD1} mice were used as controls. All mice were bred at the animal facility of the Leiden University Medical Center. Mice were housed in individually ventilated cages with a standard 12h/12h light/dark cycle. Standard rodent chow and water were available ad libitum. All experiments were approved by the Animal Experiments Committee of the LUMC.

Smchd1$^{fl/fl}$ mice and Smchd1$^{Del/+}$ mice

A Smchd1 targeting construct that introduced loxP sites surrounding exon 4 of Smchd1 and a neomycin cassette flanked by Frt sites was produced by recombineering. The targeting construct was electroporated into Bruce4 C57BL/6 embryonic stem cells. Neomycin-resistant clones were screened by Southern blot for their integrations at the 5' and 3' ends, using PCR amplified probes (5'-probe amplified with 5'-CTAAGCCCAGAACCTTG CAC-3' and 5'-CTTGAAAGCAGACAGGCTCA-3'; 3'-probe amplified with 5'-GCCCATTATTCCTCCAAACA-3' and 5'-GAATTTGCA TTTGGAAAGGA; each probe was cloned into a TOPO TA vector). The DNA was then cut with *Bss*SI for the 5'-probe, and with *Bss*SI, *Bgl*II, *Nco*I, and *Kpn*I for the 3'-probe. One correctly targeted clone was used to produce mice by blastocyst injection. The neomycin cassette was removed by crossing with the Rosa26-FLPe knockin mouse strain (35). The *Smchd1*^{fl} allele was maintained on a C57BL/6 background. The *Smchd1*^{Del} allele was generated by crossing with a constitutive CMV-driven Cre recombinase mouse strain (28), and was also maintained on a C57BL/6 background. All mice were produced and maintained under approval by The Walter and Eliza Hall Institute of Medical Research Animal Ethics Committee (AEC 2014.026).

D4Z4–2.5/Smchd1^{CKO} mice

Mice expressing Cre recombinase from the muscle-specific Myf5 locus have been described previously (27). The Smchd1 conditional knock-out line (Smchd1$^{fl/fl}$ mice) is described above. Progeny positive for the D4Z4–2.5 transgene, hemizygous or negative for Myf5-Cre recombinase, and homozygous for floxed Smchd1 were produced by a series of crossbreedings and identified by PCR analysis using toe DNA. Myf5-Cre recombinase was detected by PCR with the following primers: 5'-CGTAGAG CGCTGAAGAAGGTCAAC-3' (MyfkI forward), 5'-CACATTAGAAA ACCTGCCAACACC-3' (MyfkI reverse), and 5'-ACGAAGTTAT

Table 2. List of RT-PCR primers and corresponding sequences

Gene	Forward primer sequence	Reverse primer sequence
DUX4	5'-CCCAGGTACCAGCAGACC-3'	5'-TCCAGGAGATGTAACTCTAATCCA-3'
Gapdh	5'-TCCATGACAACTTTGGCATTG-3'	5'-TCACGCCACAGCTTTCCA-3'
Krt14	5'-TGCTGGATGTGAAGACAAGG-3'	5'-GGATGACTGAGAGCCAGAGG-3'
Mef2c	5'-TCCATCAGCCATTTCAACAA-3'	5'-GTTACAGAGCCGAGGTGGAG-3'
Rpl13a	5'-TGCTGCTCTCAAGGTTGTTC-3'	5'-TTCTCCTCCAGAGTGGCTGT-3'
Rpl27	5'-GCAAGAAGAAGATCGCCAAG-3'	5'-TCCAAGGGGATATCCACAGA-3'
Smchd1	5'-AAGCCCTTTGGAAATCCAGT-3'	5'-TGGGGCAGTGTGTGATTTTA-3'
Tgm1	5'-ACGACTGCTGGATGAAGAGG-3'	5'-TCAGCAAAAATGAAAGGTGTG-3'
Wfdc3	5'-CTTCCATGTCAGGAGCTGTG-3'	5'-ACCAGGATTCTGGGACATTG-3'

TAGGTCCCTCGAC-3' (Lox). Floxed Smchd1 alleles were detected by PCR with the following primers: 5'-CCATGAGAAGCAAT GTGGGA-3' (F4) and 5'- GGACAGCCAAAGTGACACAG-3' (R1). The D4Z4–2.5 transgene was detected by PCR with the following primers: 5'-CGGAGAACTGCCATTCTTTC-3' (LS 352F) and 5'-CAGCCAGAATTTCACGGAAG-3' (LS 354R). Cre-dependent deletion of sequences from the Smchd1 locus was confirmed by PCR analysis of genomic DNA isolated from gastrocnemius muscle with the following primers: 5'-TCAGGTGGTCTCGAGCCC-3' (F2) and 5'-GGACAGCCAAAGTGACACAG-3' (R1). The intact Smchd1 allele was detected by PCR using the following primers: 5'-TCAGGTGGTCTCGAGCCC-3' (F2) and 5'-TCGAGAAGTAGCTGA CAATGAA-3'(R2). A single Myf5-cre allele was shown to be sufficient for deletion of the Smchd1 floxed region, and we did not observe gender-dependent or age-dependent differences in the phenotype of animals positive or negative for the Cre insertion. All mice were bred at the animal facility of the Fred Hutchinson Cancer Research Center and maintained in accordance with the NIH Guide for the Care and Use of Experimental Animals. All experiments were approved by the Institutional Animal Care and Use Committee of the Fred Hutchinson Cancer Research Center.

Isolation and culturing of neonatal fibroblasts and keratinocytes

Neonatal mice were euthanized by decapitation followed by removal of the complete skin. Primary fibroblasts and primary keratinocytes were isolated following the protocol supplied by the manufacturer (CELLnTEC; Bioconnect, Huissen, the Netherlands). In short, the skin of the mice was removed, followed by overnight incubation in a dispase solution containing antibiotics and antimycotics (CELLnTEC; Bioconnect, Huissen, the Netherlands). The next day, the epidermis and dermis were separated using forceps. The dermis was next cut into small pieces and distributed over a 60 mm dish with addition of a small amount of DMEM/F12 medium (Thermo Fisher Scientific, Bleiswijk, the Netherlands) supplemented with 1% penicillin–streptomycin (Sigma Aldrich, Zwijndrecht, the Netherlands) and 20% heat-inactivated foetal bovine serum (Thermo Fisher Scientific, Bleiswijk, the Netherlands). Over the course of the week, primary fibroblasts grew out of the dermis pieces. Upon confluence, the cells were transferred to a 100 mm dish and the dermis pieces were discarded. The epidermis was incubated for 20–30 min at room temperature in Accutase (CELLnTEC; Bioconnect, Huissen, the Netherlands). After this incubation step, the epidermis was gently rubbed in a 60 mm dish to obtain single cells. These cells were then centrifuged for 5 min at room temperature and seeded at a density of 4×10^4 cells/cm^2 in a 6-well plate containing CnT-PR medium (CELLnTEC; Bioconnect, Huissen, the Netherlands). One day before confluence, cells were either harvested (proliferating keratinocytes) or the medium was changed to CnT-PR-D medium (CELLnTEC; Bioconnect, Huissen, the Netherlands). At confluence, 1.2 mM $Ca2^+$ was added to the medium to drive differentiation. Differentiated keratinocytes were harvested 7 days after changing the medium to CnT-PR-D medium.

Isolation and culturing of EDL single muscle fibres

Mice were euthanized by cervical dislocation followed by dissection of the EDL muscle from tendon to tendon. Next, the EDL muscle was digested twice in 0.2% collagenase (Sigma Aldrich, Zwijndrecht, the Netherlands) in DMEM medium (Thermo Fisher Scientific, Bleiswijk, the Netherlands) supplemented with 1% penicillin-streptomycin (Sigma Aldrich, Zwijndrecht, the Netherlands) at 37°C for 105 and 120 min, respectively. The resulting fibres were dissociated using Pasteur pipettes with different apertures, followed by several washing steps as described previously (36). Next, 150 individual fibres were cultured on matrigel-coated (BD, Breda, the Netherlands) 6-well plates in DMEM medium supplemented with 30% foetal bovine serum, 10% horse serum, 1% penicillin-streptomycin, 1% chicken embryo extract, and 2.5 ng/ml fibroblast growth factor (all Thermo Fisher Scientific, Bleiswijk, the Netherlands). The fibres were detached and removed after 3 days. The attached myoblasts were trypsinised, counted, and plated for experiments. Differentiation of myoblasts into myotubes was induced after 48 h by replacing the original medium with DMEM medium supplemented with 2% horse serum and 1% penicillin-streptomycin (both Thermo Fisher Scientific, Bleiswijk, the Netherlands). At the same time, myoblasts were harvested. 48 h post-differentiation, myotubes were harvested.

Quantitative DNA methylation analysis by bisulphite conversion sequencing

Bisulphite treatment was performed on 400 ng of genomic DNA isolated from mouse tail and we used the EZ DNA Methylation-Lightning kit (Zymo Research; BaseClear Lab Products, Leiden, the Netherlands). DNA methylation levels of the D4Z4–2.5 transgene were quantified by PCR analysis using the following primers: 5'-ATAGGGAGGGGGTATTTTA-3' and 5'-ACRATCAAAAAC ATACCTCTATCTA-3' (25). Next, the PCR product was ligated into the TOPO TA vector (Thermo Fischer Scientific, Bleiswijk, the Netherlands), followed by transformation of the ligation product in DH5α bacteria, and Sanger sequencing of plasmid DNA isolated from individual colonies. 10 individual colonies

were picked for each DNA sample and sent for Sanger sequencing.

Smchd1 and histone ChIP analyses

We followed a previously published protocol with minor modifications (37). In short, confluent cultures of neonatal fibroblasts (three 150 mm plates) were crosslinked in 1% formaldehyde for 10 min at room temperature followed by quenching of the reaction with 125 mM glycine for 5 min at room temperature. Next, crosslinked cells were lysed in NP buffer [150 mM NaCl, 50 mM Tris-HCl (pH 7.5), 5 mM EDTA, 0.5% NP-40, 0.1% Triton X-100] and the resulting chromatin was sheared using a sonicator bath (Bioruptor Pico; Diagenode, Ougrée, Belgium) for 30 min at maximum output and 30 s on/off cycles. Shearing of DNA fragments between 200–2000 bp was confirmed through phenol-chloroform extraction and agarose gel electrophoresis. DNA concentrations were determined with a Nanodrop ND-1000 spectrophotometer (Thermo Fisher Scientific, Bleiswijk, the Netherlands). For Smchd1 ChIP analysis, 30 μg of chromatin was first precleared for 1 h with blocked protein A Sepharose beads (GE Healthcare, Eindhoven, The Netherlands) followed by overnight incubation with a Smchd1 antibody (5 μg of ab31865; Abcam, Cambridge, United Kingdom) or with mouse IgG (5 μg; Diagenode, Ougrée, Belgium). For histone ChIP analysis, 3 μg of chromatin was precleared and we used the following antibodies: H3K4me2 (5 μg of 39141; Active Motif, Carlsbad, USA), H3K9me3 (5 μg of 39161; Active Motif, Carlsbad, USA), and mouse IgG (5 μg; Diagenode, Ougrée, Belgium). Immunoprecipitation was performed with 20 μl blocked sepharose A beads per reaction, and washing was performed according to the previously published protocol (37). Finally, DNA was isolated using Chelex resin (Bio-Rad, Veenendaal, the Netherlands) and diluted 1: 1 for quantitative analysis by RT-PCR. We used the following primers to amplify the D4Z4 repeat array: 5'- CCGCGTCCGTCCGTGAAA-3' and 5'-TCCGTCGCCGTCCTCGTC-3' (9).

RNA isolation and cDNA synthesis

Total RNA was isolated from different mouse tissues and cells using the miRNeasy kit (Qiagen, Venlo, the Netherlands) according to the manufacturer's instructions and included a DNase treatment. RNA concentrations were determined with a Nanodrop ND-1000 spectrophotometer (Thermo Fisher Scientific, Bleiswijk, the Netherlands). 1–3 μg of total RNA was reverse transcribed using the RevertAid H Minus First Strand cDNA synthesis kit with Oligo(dT)18 primers (both Thermo Fisher Scientific, Bleiswijk, the Netherlands), according to the instructions of the manufacturer. The resulting cDNA was treated with 2 units of RNaseH (Thermo Fisher Scientific, Bleiswijk, the Netherlands) at 37°C for 20 min and diluted in 100 μl H_2O. 2–5 μl of the diluted cDNA was used for quantitative RT-PCR analysis.

Quantitative RT-PCR analysis

RT-PCR analysis was performed in duplicate using the CFX96 system (Bio-Rad, Veenendaal, the Netherlands) with SYBR green mastermix and 0.5 pM of each primer in a 15 μl final reaction volume. All primers, spanning at least one intron, were designed using Primer3 software. Primer sequences for all reactions are listed in Table 2. The following cycling conditions were used: an initial denaturation step at 95°C for 3 min followed by 40 cycles of 10 s at 95°C and 45 s at primer Tm. Next, a melting curve analysis was performed to determine the specificity of all reactions. This analysis consisted of an initial denaturation step at 95°C for 3 min followed by 1 min incubation step at 65°C and sequential temperature increments of 0.5°C from 65–95°C. Results were analysed with Bio-Rad CFX Manager version 3.1 (Bio-Rad, Veenendaal, the Netherlands) and normalized to the reference gene Rpl27 (Fig. 3F and G) or to the reference genes Gapdh and Rpl13a (all other figures) to correct for cDNA input.

Flow cytometry of the GFP3C transgene

Mice were tailed at three weeks of age and a drop of blood was diluted in PBS. Flow cytometry was next performed to analyse GFP expression in red blood cells (20). All mice analysed were hemizygous for the GFP3C transgene, and the GFP3C line of mice has been backcrossed for more than 10 generations from FVB/N background to C57BL/6 background.

Smchd1 Western blot

Whole E12.5 embryos were harvested from intercrosses between $Smchd1^{Del/+}$ mice. Embryo tail DNA was used for genotyping. Embryos were lysed and prepared for western blot as described previously (38). Smchd1 was detected with two different Smchd1 antibodies (Bethyl labs A302–871A at 1/2000 dilution or Abcam ab31865 at 1/2000 dilution). An actin antibody was included as a control (Santa Cruz sc1616 at 1/1000 dilution).

H&E staining of skeletal muscles

Skeletal muscles were dissected and frozen in isopentane cooled to −165°C. Next, five-micron cryosections were cut, followed by H&E staining consisting of a 5 min incubation in haematoxylin, 1 min incubation in eosin, and several washing steps with dH_2O, ethyl alcohol, and xylene. H&E-stained sections were analysed by light microscopy (Leica Microsystems B.V., Rijswijk, the Netherlands).

DUX4 staining of muzzle skin

Muzzle skins were dissected and frozen in isopentane cooled to −165°C. Cryosections were cut at 5 μm thickness and placed on Superfrost Plus glasses (Thermo Fisher Scientific, Bleiswijk, the Netherlands). The sections were fixed with 4% formaldehyde in PBS for 10 min at room temperature and washed three times in PBS/0.5% Tween for 5 min. Next, the samples were blocked with 10% normal goat serum (Agilent, Amstelveen, the Netherlands) for 30 min and incubated with primary rabbit DUX4 antibody directed against the C-terminal region of DUX4 (E5.5; 1: 300 in PBS/0.1% BSA) (39). After a triple wash in PBS/0.5% Tween for 3 min, Alexa 488 donkey anti-rabbit (Thermo Fisher Scientific, Bleiswijk, the Netherlands; diluted 1: 100 in PBS/0.1%BSA) was applied for 30 min in the dark. The excess was removed by a triple PBS/0.5% Tween wash. Finally, the sections were incubated with PBS/dapi (500 ng/ml) for 15 min in the dark, washed 3 min with PBS/0.5% Tween and mounted with Aqua Poly/Mount (Polysciences Europe GmbH, Hirschberg an der Bergstrasse, Germany). The stained sections were analysed on a Leica DMRA2 microscope (Leica Microsystems B.V., Rijswijk, the Netherlands).

Histopathological examination

Complete necropsy was performed on mice that were 15 days or 9 weeks of age. Next, tissues were fixed in 4% neutral buffered formalin, and bone tissues were subjected to an additional decalcification step by incubation in formic acid for 5 days. Successively, all tissues were embedded in paraffin, sectioned at five micron, stained with H&E, and evaluated by light microscopy following standard procedures (40,41).

Flow cytometry of thymocytes

Single cell suspensions of thymocytes were obtained by homogenization of the thymus over 70 μm strainers (VWR International B.V., Amsterdam, the Netherlands). Cells were washed with phosphate-buffered saline containing 2% foetal bovine serum and subsequently stained with αCD8α-Efluor450, αCD4-PerCP-Cy5.5, αCD25-PE and αCD44-APC (all Thermo Fisher Scientific, Bleiswijk, the Netherlands) for 20 min at 4°C. After an additional washing step, flow cytometry was performed on a Canto II instrument (Becton Dickinson B.V., Vianen, the Netherlands) and analysed using FlowJo software (Becton Dickinson B.V., Vianen, the Netherlands).

Statistical analysis

Statistical analysis was performed using GraphPad Prism software (version 7.00; GraphPad Software, Inc., La Jolla, USA). Most data sets were compared using unpaired Student's *t*-tests or Mann–Whitney *U* tests, depending on whether the data were normally distributed (normality was determined by Shapiro-Wilk normality tests). The D4Z4 DNA methylation levels were compared using Student's *t*-tests; multiple testing correction was performed by Holm-Sidak multiple comparison tests. Genotype and gender distribution was tested by Pearson's chi-squared test. Body weight was tested by one-way analysis of variance (ANOVA) followed by Tukey post hoc test. Percentage of different cell populations in the thymus was tested by two-way ANOVA followed by Holm-Sidak multiple comparison tests.

Acknowledgements

We thank Saskia Maas (Department of Anatomy & Embryology, Leiden University Medical Center, Leiden, the Netherlands) for assistance with preparation of histology material. We thank Prof. Dr. Jelle Goeman (Department of Medical Statistics and Bioinformatics, Leiden University Medical Center, Leiden, the Netherlands) for statistical advice.

Conflict of Interest statement. None declared.

Funding

National Institutes of Health (NINDS: PO1 NS069539; NIAMS: RO1 AR066248), the Prinses Beatrix Spierfonds (W.OR14–24), and the Australian National Health and Medical Research Council (GNT1098290). FSH Society and FSHD Canada Foundation research fellowship (FSHS-22015–02) to YH. Bellberry-Viertel Senior Medical Research fellowship to MEB. Work performed at WEHI was also supported by Victorian State Government Operational Infrastructure Support, an NHMRC IRIISS grant (9000220).

References

1. Snider, L., Geng, L.N., Lemmers, R.J., Kyba, M., Ware, C.B., Nelson, A.M., Tawil, R., Filippova, G.N., van der Maarel, S.M., Tapscott, S.J. *et al.* (2010) Facioscapulohumeral dystrophy: incomplete suppression of a retrotransposed gene. *PLoS Genet.*, **6**, e1001181.
2. Hendrickson, P.G., Doráis, J.A., Grow, E.J., Whiddon, J.L., Lim, J.W., Wike, C.L., Weaver, B.D., Pflueger, C., Emery, B.R., Wilcox, A.L. *et al.* (2017) Conserved roles of mouse DUX and human DUX4 in activating cleavage-stage genes and MERVL/HERVL retrotransposons. *Nat. Genet.*, **49**, 925–934.
3. Whiddon, J.L., Langford, A.T., Wong, C.J., Zhong, J.W. and Tapscott, S.J. (2017) Conservation and innovation in the DUX4-family gene network. *Nat. Genet.*, **49**, 935–940.
4. De Iaco, A., Planet, E., Coluccio, A., Verp, S., Duc, J. and Trono, D. (2017) DUX-family transcription factors regulate zygotic genome activation in placental mammals. *Nat. Genet.*, **49**, 941–945.
5. Wijmenga, C., Hewitt, J.E., Sandkuijl, L.A., Clark, L.N., Wright, T.J., Dauwerse, H.G., Gruter, A.M., Hofker, M.H., Moerer, P. and Williamson, R. (1992) Chromosome 4q DNA rearrangements associated with facioscapulohumeral muscular dystrophy. *Nat. Genet.*, **2**, 26–30.
6. van Deutekom, J.C., Wijmenga, C., van Tienhoven, E.A., Gruter, A.M., Hewitt, J.E., Padberg, G.W., van Ommen, G.J., Hofker, M.H. and Frants, R.R. (1993) FSHD associated DNA rearrangements are due to deletions of integral copies of a 3.2 kb tandemly repeated unit. *Hum. Mol. Genet.*, **2**, 2037–2042.
7. Lemmers, R.J., Wohlgemuth, M., van der Gaag, K.J., van der Vliet, P.J., van Teijlingen, C.M., de Knijff, P., Padberg, G.W., Frants, R.R. and van der Maarel, S.M. (2007) Specific sequence variations within the 4q35 region are associated with facioscapulohumeral muscular dystrophy. *Am. J. Hum. Genet.*, **81**, 884–894.
8. van Overveld, P.G., Lemmers, R.J., Sandkuijl, L.A., Enthoven, L., Winokur, S.T., Bakels, F., Padberg, G.W., van Ommen, G.J., Frants, R.R. and van der Maarel, S.M. (2003) Hypomethylation of D4Z4 in 4q-linked and non-4q-linked facioscapulohumeral muscular dystrophy. *Nat. Genet.*, **35**, 315–317.
9. Zeng, W., de Greef, J.C., Chen, Y.Y., Chien, R., Kong, X., Gregson, H.C., Winokur, S.T., Pyle, A., Robertson, K.D., Schmiesing, J.A. *et al.* (2009) Specific loss of histone H3 lysine 9 trimethylation and HP1gamma/cohesin binding at D4Z4 repeats is associated with facioscapulohumeral dystrophy (FSHD). *PLoS Genet.*, **5**, e1000559.
10. Jones, T.I., Chen, J.C., Rahimov, F., Homma, S., Arashiro, P., Beermann, M.L., King, O.D., Miller, J.B., Kunkel, L.M., Emerson, C.P., Jr. *et al.* (2012) Facioscapulohumeral muscular dystrophy family studies of DUX4 expression: evidence for disease modifiers and a quantitative model of pathogenesis. *Hum. Mol. Genet.*, **21**, 4419–4430.
11. Lemmers, R.J., Tawil, R., Petek, L.M., Balog, J., Block, G.J., Santen, G.W., Amell, A.M., van der Vliet, P.J., Almomani, R., Straasheijm, K.R. *et al.* (2012) Digenic inheritance of an SMCHD1 mutation and an FSHD-permissive D4Z4 allele causes facioscapulohumeral muscular dystrophy type 2. *Nat. Genet.*, **44**, 1370–1374.
12. van den Boogaard, M.L., Lemmers, R.J., Balog, J., Wohlgemuth, M., Auranen, M., Mitsuhashi, S., van der Vliet, P.J., Straasheijm, K.R., van den Akker, R.F., Kriek, M. *et al.* (2016) Mutations in DNMT3B modify epigenetic repression of the D4Z4 repeat and the penetrance of facioscapulohumeral dystrophy. *Am. J. Hum. Genet.*, **98**, 1020–1029.

13. Sacconi, S., Lemmers, R.J., Balog, J., van der Vliet, P.J., Lahaut, P., van Nieuwenhuizen, M.P., Straasheijm, K.R., Debipersad, R.D., Vos-Versteeg, M., Salviati, L. *et al.* (2013) The FSHD2 gene SMCHD1 is a modifier of disease severity in families affected by FSHD1. *Am. J. Hum. Genet.*, **93**, 744–751.
14. Larsen, M., Rost, S., El Hajj, N., Ferbert, A., Deschauer, M., Walter, M.C., Schoser, B., Tacik, P., Kress, W. and Müller, C.R. (2015) Diagnostic approach for FSHD revisited: SMCHD1 mutations cause FSHD2 and act as modifiers of disease severity in FSHD1. *Eur. J. Hum. Genet.*, **23**, 808–816.
15. Krom, Y.D., Thijssen, P.E., Young, J.M., den Hamer, B., Balog, J., Yao, Z., Maves, L., Snider, L., Knopp, P., Zammit, P.S. *et al.* (2013) Intrinsic epigenetic regulation of the D4Z4 macrosatellite repeat in a transgenic mouse model for FSHD. *PLoS Genet.*, **9**, e1003415.
16. Wallace, L.M., Garwick, S.E., Mei, W., Belayew, A., Coppee, F., Ladner, K.J., Guttridge, D., Yang, J. and Harper, S.Q. (2011) DUX4, a candidate gene for facioscapulohumeral muscular dystrophy, causes p53-dependent myopathy in vivo. *Ann. Neurol.*, **69**, 540–552.
17. Bosnakovski, D., Chan, S.S.K., Recht, O.O., Hartweck, L.M., Gustafson, C.J., Athman, L.L., Lowe, D.A. and Kyba, M. (2017) Muscle pathology from stochastic low level DUX4 expression in an FSHD mouse model. *Nat. Commun.*, **8**, 550.
18. Tassin, A., Laoudj-Chenivesse, D., Vanderplanck, C., Barro, M., Charron, S., Ansseau, E., Chen, Y.W., Mercier, J., Coppée, F. and Belayew, A. (2013) DUX4 expression in FSHD muscle cells: how could such a rare protein cause a myopathy?. *J. Cell. Mol. Med.*, **17**, 76–89.
19. Balog, J., Thijssen, P.E., Shadle, S., Straasheijm, K.R., van der Vliet, P.J., Krom, Y.D., van den Boogaard, M.L., de Jong, A., Lemmers, R.J., Tawil, R. *et al.* (2015) Increased DUX4 expression during muscle differentiation correlates with decreased SMCHD1 protein levels at D4Z4. *Epigenetics*, **10**, 1133–1142.
20. Blewitt, M.E., Vickaryous, N.K., Hemley, S.J., Ashe, A., Bruxner, T.J., Preis, J.I., Arkell, R. and Whitelaw, E. (2005) An N-ethyl-N-nitrosourea screen for genes involved in variegation in the mouse. *Proc. Natl. Acad. Sci. U. S. A*, **102**, 7629–7634.
21. Blewitt, M.E., Gendrel, A.V., Pang, Z., Sparrow, D.B., Whitelaw, N., Craig, J.M., Apedaile, A., Hilton, D.J., Dunwoodie, S.L., Brockdorff, N. *et al.* (2008) SmcHD1, containing a structural-maintenance-of-chromosomes hinge domain, has a critical role in X inactivation. *Nat. Genet.*, **40**, 663–669.
22. Mould, A.W., Pang, Z., Pakusch, M., Tonks, I.D., Stark, M., Carrie, D., Mukhopadhyay, P., Seidel, A., Ellis, J.J., Deakin, J. *et al.* (2013) Smchd1 regulates a subset of autosomal genes subject to monoallelic expression in addition to being critical for X inactivation. *Epigenetics Chromatin*, **6**, 19.
23. Gendrel, A.V., Tang, Y.A., Suzuki, M., Godwin, J., Nesterova, T.B., Greally, J.M., Heard, E. and Brockdorff, N. (2013) Epigenetic functions of smchd1 repress gene clusters on the inactive X chromosome and on autosomes. *Mol. Cell. Biol.*, **33**, 3150–3165.
24. Dandapat, A., Bosnakovski, D., Hartweck, L.M., Arpke, R.W., Baltgalvis, K.A., Vang, D., Baik, J., Darabi, R., Perlingeiro, R.C., Hamra, F.K. *et al.* (2014) Dominant lethal pathologies in male mice engineered to contain an X-linked DUX4 transgene. *Cell Rep.*, **8**, 1484–1496.
25. Calandra, P., Cascino, I., Lemmers, R.J., Galluzzi, G., Teveroni, E., Monforte, M., Tasca, G., Ricci, E., Moretti, F., van der Maarel, S.M. *et al.* (2016) Allele-specific DNA hypomethylation characterises FSHD1 and FSHD2. *J. Med. Genet.*, **53**, 348–355.
26. Balog, J., Thijssen, P.E., de Greef, J.C., Shah, B., van Engelen, B.G., Yokomori, K., Tapscott, S.J., Tawil, R. and van der Maarel, S.M. (2012) Correlation analysis of clinical parameters with epigenetic modifications in the DUX4 promoter in FSHD. *Epigenetics*, **7**, 579–584.
27. Tallquist, M.D., Weismann, K.E., Hellström, M. and Soriano, P. (2000) Early myotome specification regulates PDGFA expression and axial skeleton development. *Development*, **127**, 5059–5070.
28. Schwenk, F., Baron, U. and Rajewsky, K. (1995) A cre-transgenic mouse strain for the ubiquitous deletion of loxP-flanked gene segments including deletion in germ cells. *Nucleic Acids Res.*, **23**, 5080–5081.
29. Kawazu, M., Yamamoto, G., Yoshimi, M., Yamamoto, K., Asai, T., Ichikawa, M., Seo, S., Nakagawa, M., Chiba, S., Kurokawa, M. and Ogawa, S. (2007) Expression profiling of immature thymocytes revealed a novel homeobox gene that regulates double-negative thymocyte development. *J. Immunol.*, **179**, 5335–5345.
30. Wu, S.L., Tsai, M.S., Wong, S.H., Hsieh-Li, H.M., Tsai, T.S., Chang, W.T., Huang, S.L., Chiu, C.C. and Wang, S.H. (2010) Characterization of genomic structures and expression profiles of three tandem repeats of a mouse double homeobox gene: Duxbl. *Dev. Dyn.*, **239**, 927–940.
31. Knopp, P., Krom, Y.D., Banerji, C.R., Panamarova, M., Moyle, L.A., den Hamer, B., van der Maarel, S.M. and Zammit, P.S. (2016) DUX4 induces a transcriptome more characteristic of a less-differentiated cell state and inhibits myogenesis. *J. Cell Sci.*, **129**, 3816–3831.
32. Dandapat, A., Perrin, B.J., Cabelka, C., Razzoli, M., Ervasti, J.M., Bartolomucci, A., Lowe, D.A. and Kyba, M. (2016) High frequency hearing loss and hyperactivity in DUX4 transgenic mice. *PLoS One*, **11**, e0151467.
33. Gannon, O.M., Merida de Long, L. and Saunders, N.A. (2016) DUX4 Is Derepressed in late-differentiating keratinocytes in conjunction with loss of H3K9me3 epigenetic repression. *J. Invest. Dermatol.*, **136**, 1299–1302.
34. Das, S. and Chadwick, B.P. (2016) Influence of repressive histone and DNA methylation upon D4Z4 transcription in non-myogenic cells. *PLoS One*, **11**, e0160022.
35. Farley, F.W., Soriano, P., Steffen, L.S. and Dymecki, S.M. (2000) Widespread recombinase expression using FLPeR (flipper) mice. *Genesis*, **28**, 106–110.
36. Collins, C.A. and Zammit, P.S. (2009) Isolation and grafting of single muscle fibres. *Methods Mol. Biol.*, **482**, 319–330.
37. Nelson, J.D., Denisenko, O. and Bomsztyk, K. (2006) Protocol for the fast chromatin immunoprecipitation (ChIP) method. *Nat. Protoc.*, **1**, 179–185.
38. Keniry, A., Gearing, L.J., Jansz, N., Liu, J., Holik, A.Z., Hickey, P.F., Kinkel, S.A., Moore, D.L., Breslin, K., Chen, K. *et al.* (2016) Setdb1-mediated H3K9 methylation is enriched on the inactive X and plays a role in its epigenetic silencing. *Epigenetics Chromatin*, **9**, 16.
39. Geng, L.N., Tyler, A.E. and Tapscott, S.J. (2011) Immunodetection of human double homeobox 4. *Hybridoma (Larchmt)*, **30**, 125–130.
40. Morawietz, G., Ruehl-Fehlert, C., Kittel, B., Bube, A., Keane, K., Halm, S., Heuser, A. and Hellmann, J. RITA Group, NACAD Group. (2004) Revised guides for organ sampling and trimming in rats and mice–Part 3. A joint publication of the RITA and NACAD groups. *Exp. Toxicol. Pathol.*, **55**, 433–449.
41. Parkinson, C.M., O'Brien, A., Albers, T.M., Simon, M.A., Clifford, C.B. and Pritchett-Corning, K.R. (2011) Diagnostic necropsy and selected tissue and sample collection in rats and mice. *J. Vis. Exp.*, **54**, pii: 2966.